ISSN 2718-322X (Online)
ISSN 1331-7210 (Print)

Engineering Power

BULLETIN OF THE CROATIAN ACADEMY OF ENGINEERING Vol. 15(4) 2020

EDITOR-IN-CHIEF'S WORD

At the end of this year you are holding in your hands the latest fourth issue of our Engineering Power Bulletin, in which we have been regularly publishing interesting scientific topics of our renowned members for years.

This time, Prof. Saša Zelenika, PhD, full member of the Croatian Academy of Engineering, is presenting a part of his team's research work on a very scientific and engineering topic of the problems and possibilities of nanotechnology, especially microsystems in technology.

I hope that these papers will arouse your professional interest and provide you with new and useful insights.

Editor-in-Chief
Vladimir Andročec, President of the Croatian Academy of Engineering

EDITOR'S WORD

Dear readers,

It is my pleasure to present in this edition of the HATZ-Bulletin Engineering Power prominent research activities in the field of precision engineering and micro- and nanotechnologies carried out at the University of Rijeka.

The guest editor of this edition is Saša Zelenika, Member of the Academy and Professor at the Faculty of Engineering of the University of Rijeka, who presents part of the research work of the Faculty's Precision Engineering Laboratory and the Centre-for Micro- and Nanosciences and Technologies of the same university.

Editor
Zdravko Terze, Vice-President of the Croatian Academy of Engineering

FOREWORD

Precision engineering and micro- and nanotechnologies are of outmost importance in promoting engineering as a driving factor for the development of Croatian economy, since they have an enormous financial and stimulating potential for interdisciplinary R&D in manufacturing, materials science, optics, robotics, measurement technologies, ICT, energy, transportation, biomedicine or consumer goods. Indeed, they are the key enabling technologies identified in the smart specialisation strategies at EU and Croatian level, which have great potential to boost high value-added sectors of the economy fostering productivity and employment.

The potentials of precision engineering and micro- and nanotechnologies are illustrated herein through examples of the developments at the Precision Engineering Laboratory of the Faculty of Engineering (precenglab.riteh.uniri.hr) and the Centre-for Micro- and Nanosciences and Technologies (nanori.uniri.hr) of the University of Rijeka, Croatia. In this context, the activities relating to precision positioning, one of the key factors in the development of precision mechanics, are first presented. Two main mechanical engineering design approaches can hence be followed. Conventional sliding and rolling mechanisms, allowing extended motions and load capacities, can be used, but they are characterised by stochastic nonlinearities such as friction. Modelling using state-of-the-art integrative heuristic approaches, coupled with advanced mechatronics-based compensation, which is increasingly based on adaptive and machine-learning predictive control methods, must therefore be used. A valid alternative is the use of compliant mechanisms that are free of friction, backlash and wear, but have a complex kinematics with parasitic motions. Therefore, advanced nonlinear numerical modelling must be used, which enables the development of design configurations with minimised parasitic displacements and maximised stable working ranges. The developed ultrahigh-precision devices are generally based on suitable sensing elements, which are, in turn, increasingly autonomous and founded on energy harvesting principles. A section on our research on the potential applications of energy harvesting in the development of autonomous wearable devices, aimed at applications in telemedicine, patient monitoring or IoT, and based on innovative geometrical and dynamical excitation strategies applied to piezoelectric energy harvesting devices, and/or on thermogenerators, is illustrative of these trends. Many of these technological advances are based on materials technologies and the respective multidomain and multiscale effects. As an example of these advances, our activities in characterising the concurrent influence of multiple process parameters on fundamental frictional effects in the nanometric domain, is also given. State-of-the-art single asperity nanotechnological experimental technologies, coupled to the most advanced machine learning and artificial intelligence-based modelling methods, have thus to be used to obtain the functional description of the dependence of nanoscale friction on the studied variables, i.e., for nanoscale friction prediction.

All research results presented are achieved by networking our capacities at the national as well as on the European and international levels. One of the main goals of these activities is also to enhance the competencies of the early-stage researchers in our research group. In addition, the described activities are intensely disseminated via a broad range of science outreach activities.

Guest-Editor
Saša Zelenika, University of Rijeka, Faculty of Engineering & Centre for Micro- and Nanosciences and Technologies

CONTENT

Ervin Kamenar,[1, 2] *Saša Zelenika,*[1, 2] *and Marko Perčić*[1, 2]

Friction compensation in ultrahigh-precision positioning

[1] University of Rijeka, Faculty of Engineering, Vukovarska 58, 51000 Rijeka, Croatia
[2] University of Rijeka, Centre for Micro- and Nanosciences and Technologies & Center for Artificial Intelligence and Cybersecurity, Radmile Matejčić 2, 51000 Rijeka, Croatia

Abstract

Ultrahigh-precision positioning devices are essential in precision engineering and microsystems' technologies. As they need to allow sub-micrometric or even nanometric displacements, their nonlinear frictional behaviour, induced by a number of sliding and rolling components, has to be efficiently compensated for. If a model-based approach is followed, suitable modelling of such disturbances, which is generally performed using state-of the art friction models, has to be performed. An overview of different compensation and control algorithms applied to ultrahigh-precision positioning systems is hence given in this work.

Keywords: *friction compensation, ultrahigh-precision, precision engineering, microsystem technologies, control algorithms*

1. Introduction

Ultrahigh-precision positioning systems are important devices in microsystems' technologies and precision engineering in general, and particularly in machine tools, optics, robotics and production of semiconductors [1]. Such devices typically enable achieving positioning precisions in the micrometric or even nanometric domains. Due to a number of sliding and rolling machine elements in relative motion, these mechatronics systems are usually subject to different nonlinear dynamical effects that negatively affect their positioning performances. The dominant disturbance in this frame is the time-, position- and temperature-dependent friction, with its nonlinear stochastic characteristics. Frictional disturbances have thus to be compensated for via appropriate control algorithms. If a model-based approach is followed, the first crucial step is to properly model frictional disturbances and then, based on the required positioning performances, implement appropriate control algorithms. The majority of available literature suggests that the frictional behaviour can be represented by friction models that consider two typical motion regimes: gross sliding and pre-sliding. Recent studies show, however, that these models could be improved further by extending them to the nanometric domain [2]. There are also some emerging non-model based approaches, which could be efficiently used in some of the considered cases.

Various friction compensation techniques and control algorithms for precision positioning devices are hence presented in this work. These approaches are briefly introduced, their main characteristics and performances are described, and experimental results from previous work of the same authors are presented and discussed.

2. Friction modelling

Friction effects are usually referred to two motion regimes in the literature: the pre-sliding and the (gross) sliding regime. Recently, experiments shownhave shown that ultrahigh-precision positioning certainly happens in the pre-sliding motion regime. It is thus important to account for this effect when developing suitable model-based control methods [1].

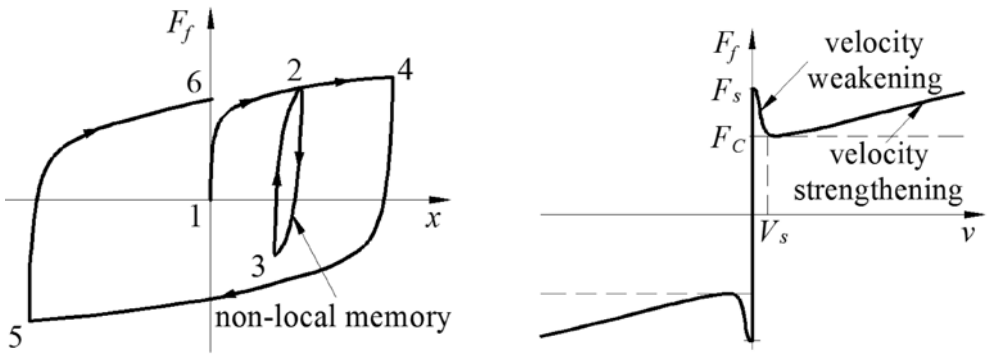

Fig. 1. Friction in the pre-sliding (left) and in the sliding (right) motion regimes

The pre-sliding motion regime is characterized by an elastoplastic nonlinear behaviour with hysteresis that depends on normal and tangential forces as well as on the history of motion (Figure 1 left). What is more, hysteresis is characterized here by non-local memory, i.e., an input-output relationship such that, when there are multiple displacement reversals, at each closure of the inner loop, the curve of the outer loop is followed again [3]. It should be noted that the frictional behaviour at the nanometric level [2] is treated in detail in a separate contribution below, and will thus not be considered further in the examples presented in this work.

In the pre-sliding motion regime, friction is a function of displacement rather than velocity. As the displacement increases, friction becomes a function of velocity, i.e. enters the sliding motion regime where it is characterized by static friction, Coulomb friction and viscous friction, i.e., it can be described by the conventional Stribeck friction curve (Figure 1 right).

The described frictional effects can be characterized by different state-of-the-art friction models [3-4]. One of the most comprehensive and widely used friction models is the Generalized Maxwell Slip (GMS) model [5] (Figure 2). This model enables taking into account both motion regimes and all the important frictional effects depicted in Figure 1, and can hence be used for model-based control schemes that are suitable to achieve ultrahigh-precision positioning. In order to apply such a model to precision positioning system, their characteristic parameters have, however, to be identified experimentally. A detail description of the experimental procedure aimed at the identification of frictional parameters is given in [1, 4].

3. Compensation strategies

In the following sections, different friction compensation approaches, some of them being model-based and some non-model based, are presented.

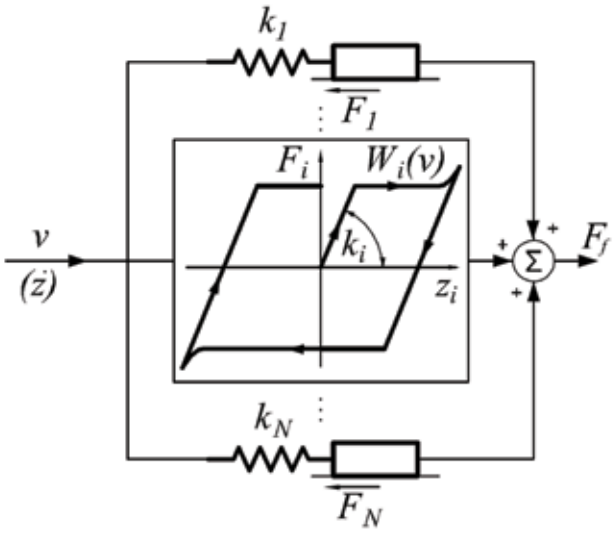

Fig. 2. The GMS friction model

3.1. Conventional PID control and the feed-forward approaches

The PID controller is a widely used control approach in many industrial environments. This feedback control method multiplies the value of the error, determined as the difference between a set-point and the process value, by proportional, integral and derivative gains commonly determined via a trial-and-error procedure or the Ziegler-Nichols tuning rules [3]. The PID controller gains are typically tuned for a determined motion regime and cannot, therefore, assure the same level of accuracy for different motion amplitudes. What is more, the optimal PID gains can vary even for the same motion amplitude, but in different positions on the considered motion mechanism. It is thus obvious that, although PID controllers allow building control laws even without developing a complete mathematical model of the positioning system, generally they do not allow compensating efficiently for the effects induced by frictional disturbances [3].

Since PID-based control approaches cannot, thus, account for stochastic frictional effects present in ultrahigh-

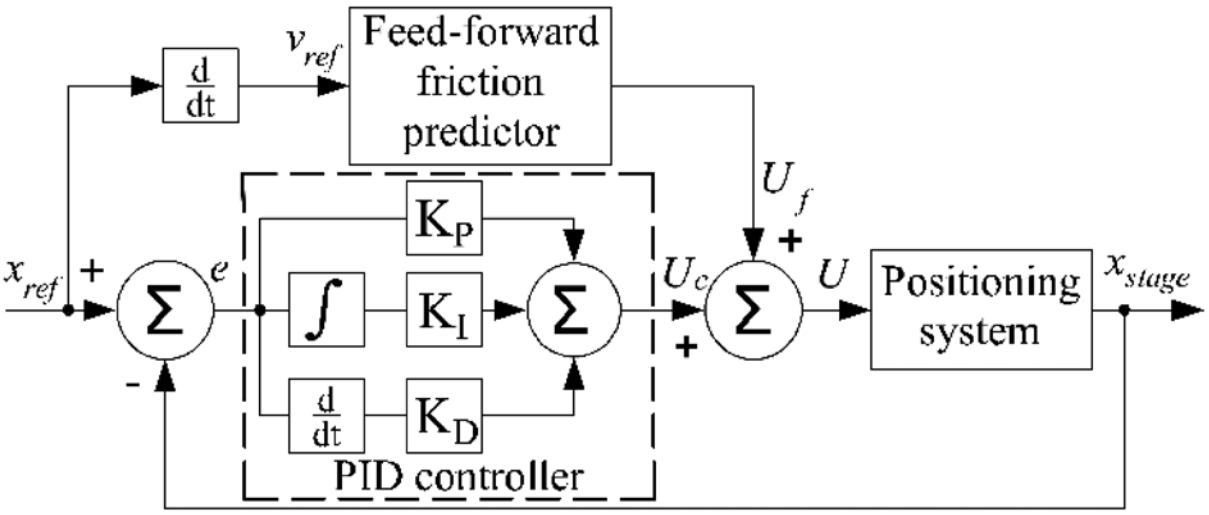

Fig. 3. The control algorithm based on feed-forward compensation of frictional disturbances and a PID

precision positioning systems, PID can be enhanced by employing an additional feed-forward term, which is based on the friction model of the system (Figure 3) [3]. It was, in fact, recently shown that a conventional PID controller, complemented with a feed-forward term based on the Generalized Maxwell-slip friction model, guarantees positioning performances in the sub-micrometric domain. On the other hand, however, the real-time implementation of the resulting controller can be quite challenging [3].

3.2. Cascade control

Cascade controllers are typically made of two PI controllers in series, one of which closes the velocity and the other one the position loop. It was experimentally shown that the cascade control can be efficiently used for positioning control, although the tuning of the parameters of two PI controllers can be difficult as well as computationally quite intensive [6]. This limits the execution time, which directly affects systems' dynamic response. As in the case of the PID controller alone, another disadvantage of this approach is that its gains are typically tuned for a certain motion regime and/or a certain position on the considered motion mechanism, and therefore it cannot assure the same level of accuracy for different motion amplitudes and/or different positions.

3.3. Model reference adaptive control

The aim of the work performed in [7] was to develop a model-based adaptive control approach based on pulse width modulation (PWM). The coefficient of proportionality between the pulse width and the respective displacement is determined here adaptively by using the model reference adaptive control (MRAC) algorithm (Figure 4). The resulting displacement of the system, based on the characteristic equation implemented in the regulator, is hence determined by a parameter adaptation algorithm (PAA).

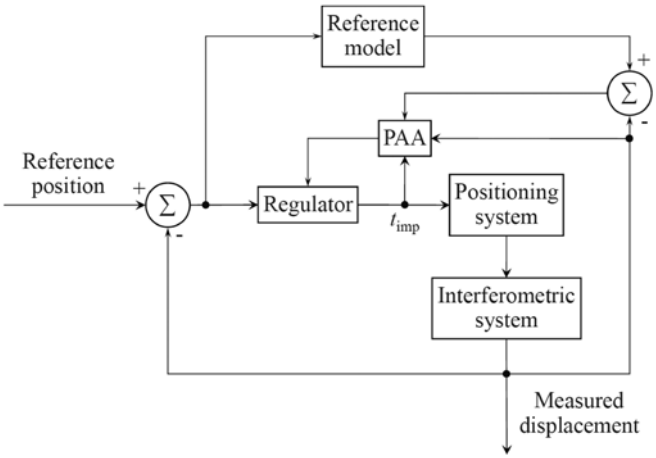

Fig. 4. Model reference adaptive control approach

In [7] it was shown that, for pulse widths of 200 ms or less, i.e., for high-precision (pre-sliding) displacements limited to approximately 10 μm, a proposed quadratic relation describes excellently the behaviour of the used positioning system. When displacement amplitudes larger than the limit of validity of the quadratic relation are needed, a simple P control is then used to bring the stage within the range of validity of the MRAC, i.e., the overall positioning algorithm is structured as a dual control algorithm. In the experimental validation, the developed approach allowed obtaining positioning performances in the sub-micrometric domain. However, its applicability is limited not only by the characteristic marked overshoots of the P controller, but particularly by a considerable lowering of the positioning speed, especially for longer travel ranges, when a suitable

switching element between the P and the MRAC-based PWM has to be used [7].

3.4. Self-tuning regulators

In the set of available adaptive nonlinear control schemes, self-tuning regulators (STR) are a viable and simple solution for stochastic systems. An example of such a controller is a self-tuning PID controller whose gains are tuned online based on the theory of adaptive interactions (Figure 5).

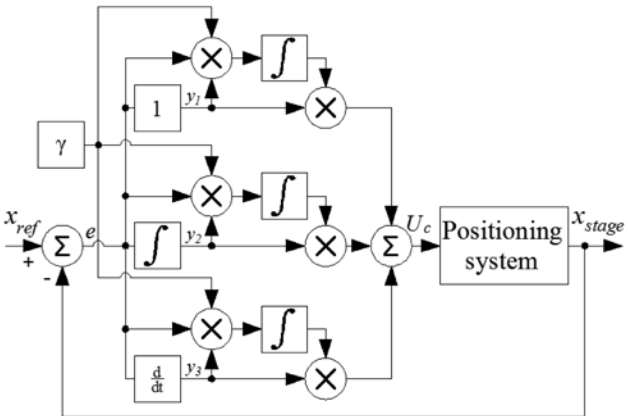

Fig. 5. PID self-tuning regulator block-diagram

In its simplified form, the STR algorithm does not depend on the plant model, while the adaptation of the parameters of the regulator can be reduced to an algorithm based on a single adaptation coefficient γ. Experiments show that, although this algorithm is able to guarantee very small steady-state errors, in point-to-point positioning it can induce quite large overshoots (Figure 6) [3].

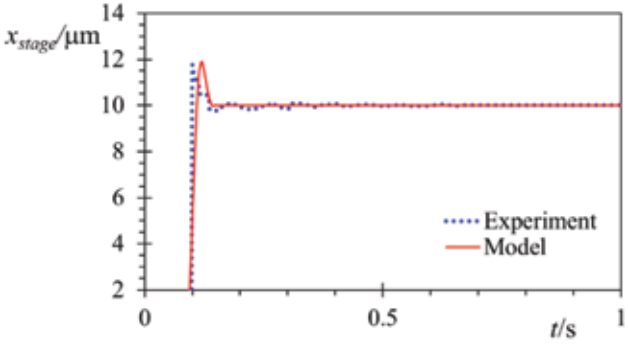

Fig. 6. Point-to-point performances of a precision positioning system controlled via an STR approach

3.5. State-space control methods

In [6] a state-space controller based on a vector with two gains is synthetized by using the pole placement method, i.e., by employing Ackerman's formula with an additional gain used to minimize steady-state errors. The positioning performances of such a controller are compared to that of the PID and of the cascade regulators (Figure 7). It was hence concluded that this control algorithm allows lowering the overshoot and the rise time compared to those attained via the PID and the cascade control methods.

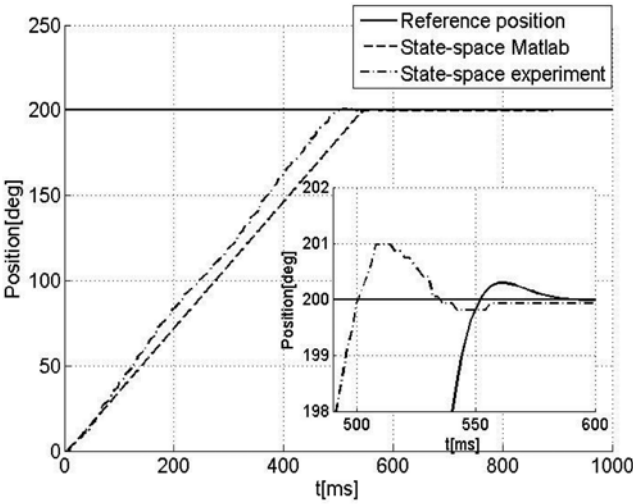

Fig. 7. Performance comparison for different algorithms

It is to be noted in this frame that, if the state-space model of the system is known, other methods, such as the linear quadratic regulator (LQR) or the model predictive control (MPC), could be employed to obtain the vector of gains.

Besides using a classical approach to build the system's state-space model, i.e., by writing the respective differential equations as described in [6], a data-driven approach can also be followed, as it will be shown in the following section.

3.6. Koopman Model Predictive Control (MPC)

The Koopman operator represents a mathematical tool that can be applied to estimate the behaviour (i.e., the future states) of a nonlinear dynamical system. Recently the Koopman operator, whose numerical approximations allow "lifting" the nonlinear dynamics of the considered device (i.e., of its state-space model) into a higher dimensional space - where its behaviour can be accurately predicted by a linear system, was, in fact, successfully extended to controlled dynamic systems [8] and applied to ultrahigh-precision positioning [9].

What is particularly important is that this scheme does not require the mathematical description of the observed system, i.e., it is completely data-driven, and therefore it reduces to a nonlinear transformation of the data (the lifting) and a linear least squares problem in the lifted space. What is more, such linear predictors have shown superior prediction performances compared to e.g. local linearization procedures. The obtained predictors have

been then recently also successfully used in the design of Model Predictive Controllers (MPCs) for nonlinear dynamical systems, with the resultant computational complexity comparable to that of MPCs for linear dynamical systems [8-9]. The same approach can then be also used to design other types of controllers, such as, for example, the Linear Quadratic Regulator (LQR) or the H-infinity method (H∞), again based on the state-space model built from measured data only. In fact, MPCs are an emerging class of algorithms based on an iterative optimization of the model of the considered devices subject to constraints, by allowing the time frame of the behaviour of the device to be extended to a finite future time horizon (prediction), which is increasingly used in industrial settings.

The Koopman operator is therefore applied in [9] to track the position of an ultrahigh-precision positioning device. The open loop response of this system, obtained for a random input, is depicted in Figure 8. It can thus be seen that the Koopman operator allows obtaining a state-space model of the system that follows very accurately the real dynamics of the system.

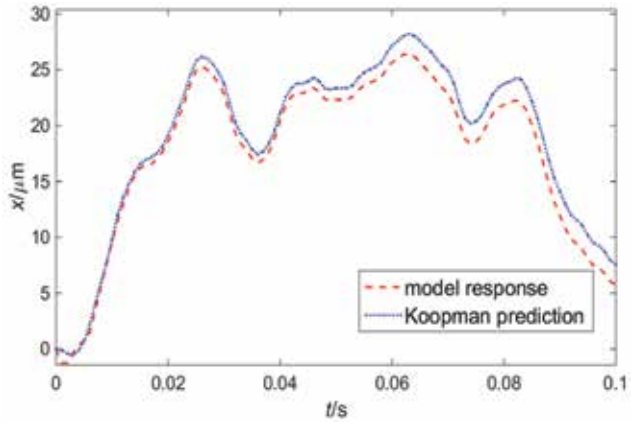

Fig. 8. Prediction of the Koopman-based model of the behaviour of an ultrahigh-precision positioning system

A further investigation of the closed-loop responses of the system controlled with different approaches was performed [9]. In the first set of experiments, the positioning device follows a sinusoidal trajectory (Figure 9).

It can hence be seen that the largest tracking error is induced by the PID controller. When PID is complemented with a feed-forward (FF) term, the tracking error is reduced, but the parameters of the PID have still to be adapted to each amplitude and/or frequency change, while the slow dynamics of the controller limits its real-time implementation. When STR and Koopman MPC are used instead, the tracking errors are significantly reduced in all considered cases. It is evident, however, that STR tracks somewhat better the reference signal at direction reversals, whereas the

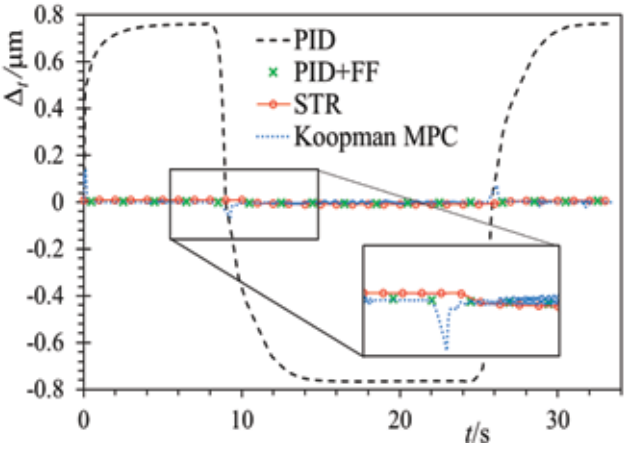

Fig. 9. Tracking errors for different control approaches

employment of the Koopman-based MPC controller induces small "glitches". It must be pointed out, however, that in the studied case the lifting map was a simple delay embedding, whereas a more elaborate choice of this map could potentially eliminate this problem [9].

A second batch of experiments is related to point-to-point positioning for Koopman-based MPC, compared to STR data used here as benchmark (Figure 10). It can thus be clearly observed that for both the STR and the Koopman-based MPC the tracking errors are very low, but in point-to-point positioning Koopman-MPC outperforms STR PID in terms of lower overshoots and shorter settling times.

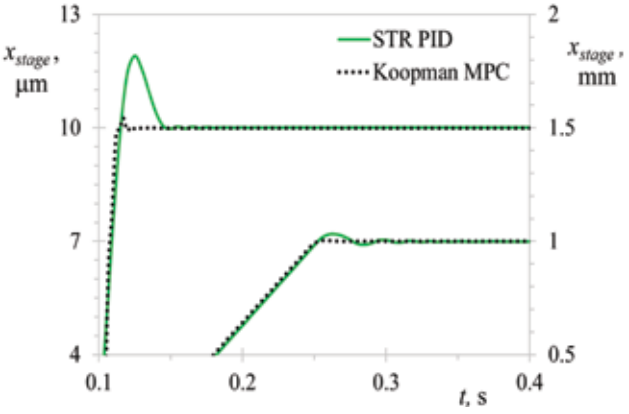

Fig. 10. Point-to-point positioning experiments for STR and Koopman-based MPC

The data-driven machine learning approach based on the Koopman operator theory was recently applied in modelling a complex pneumatically-driven soft robotic device as well. In that case, the comparison of experimental responses with those obtained from simulations on the obtained Koopman-based model, for different prediction steps, allowed establishing that the modelled responses follow again very accurately the experimental data. With the aim of allowing to attain a precise tracking control of the end-effector of the soft

robotic device, the thus developed model will be used in future work to synthetize a completely novel motion controller [10].

4. Conclusions and outlook

Different friction compensation and control approaches used in ultrahigh-precision positioning devices, starting from the PID controller which is a widely used control approach in many industrial environments, and usually does not require the model of the system, are presented in this work.

Due to the fact that the PID control typology cannot account for stochastic frictional effects present in ultrahigh-precision positioning applications, it is often complemented with an additional feed-forward term, generally established as a friction compensator based on some of the state-of-the-art friction models such as the GMS description of friction. Although the PID + FF control approach can assure high precision and accuracy levels, its real-time implementation can be quite difficult.

Furthermore, two PI controllers in a cascade arrangement can be used. This approach cannot, however, account again for the stochastic nature of friction.

One of the viable solutions is then to resort to adaptive control typologies such as the model reference adaptive control (MRAC), which proved to be efficient for ultrahigh-precision positioning, but again at the expense of its difficult real-time implementation. An example of a relatively simple adaptive control algorithm in terms of its real-time implementation, is the self-tuning regulator (STR), which is proven to be very efficient in ultrahigh-precision positioning. On the other hand, however, STR can induce overshoots in point-to-point positioning.

It was shown next that control approaches based on the state-space model of the observed system can also be very efficient in precision positioning applications. It is generally very hard, though, to obtain the mathematical models of complex devices such as some of those commonly used in ultrahigh-precision positioning applications. A recently proposed data-driven approach, based on Koopman operator theory, can, in turn, be efficiently used in this case to build a state-space model of the system, based on measured data only. The procedure of constructing the respective control algorithm is then the same as for systems with mathematical models based on differential equations. The Koopman-based technique has been applied to ultrahigh-precision positioning and similar positioning performances as in the case of the STR controller are obtained, with a marked advantage in terms of decreased overshoots and settling times in point-to-point positioning.

Due to its proven efficiency, in future work the data-driven machine learning approach based on the Koopman operator theory will thus be applied to control the positioning performances of the end-effector of pneumatically driven soft robotic devices.

Acknowledgements

This work was partly enabled by using the equipment funded via the EU European Regional Development Fund (ERDF) project no. RC.2.2.06-0001: “Research Infrastructure for Campus-based Laboratories at the University of Rijeka (RISK)”.

References

[1] Kamenar, E. (2016). *Ultra-high precision positioning via a mechatronics approach.* Doctoral dissertation, University of Rijeka, Faculty of Engineering, Rijeka (HR).

[2] Perčić, M., Zelenika, S., Mezić, I., Peter, R. and Krstulović, N. (2020). An experimental methodology for the concurrent characterization of multiple parameters influencing nanoscale friction. *Friction* 8*(3)* 577-93.

[3] Kamenar, E. & Zelenika, S. (2017). Nanometric positioning accuracy in the presence of presliding and sliding friction: Modelling, identification and compensation. *Mechanics based design of structures and machines* 45*(1)* 111-26.

[4] Kamenar, E. & Zelenika, S. (2019). Issues in validation of pre-sliding friction models for ultra-high precision positioning. *Proceedings of the Institution of Mechanical Engineers, Part C: Journal of Mechanical Engineering Science* 233*(3)* 997-1006.

[5] Al-Bender, F. & De Moerlooze, K. (2011). Characterization and modeling of friction and wear: an overview. *Sustainable Construction and Design* 2*(1)* 19.

[6] Bacac, N., Slukic, V., Puškarić, M., Stih, B., Kamenar, E. & Zelenika, S. (2014). Comparison of different DC motor positioning control algorithms. In *37th International Convention on Information and Communication Technology, Electronics and Microelectronics (MIPRO)* Opatija (HR) 1654-9.

[7] Zelenika, S. & De Bona, F. (2009). Nano-positioning using an adaptive pulse width approach. *Proceedings of the Institution of Mechanical Engineers, Part C: Journal of Mechanical Engineering Science* 223*(8)* 1955-63.

[8] Korda, M. & Mezić, I. (2018). Linear predictors for nonlinear dynamical systems: Koopman operator meets model predictive control. *Automatica* 93 149-60.

[9] Zelenika, S., Kamenar, E., Korda, M. & Mezić, I. (2020). Application of Koopman-Based Control in Ultrahigh-Precision Positioning. In *The Koopman Operator in Systems and Control – Lecture Notes in Control and Information Sciences No. 484* (Mauroy, A., Mezić, I. and Susuki, Y. ed.), Springer Nature, Heidelberg (DE) 451-79 (Chapter 17).

[10] Kamenar, E., Črnjarić-Žic, N., Haggerty, D., Zelenika, S., Hawkes, E. & Mezić, I. Prediction of the Behavior of a Pneumatic Soft Robot Based on Koopman Operator Theory. In *43rd International Convention on Information and Communication Technology, Electronics and Microelectronics (MIPRO)* Opatija (HR) 1417-21.

Kristina Marković [1, 2] *and Saša Zelenika* [1, 2]

Influence of design parameters on the behaviour of cross-spring pivots

[1] University of Rijeka, Faculty of Engineering, Vukovarska 58, 51000 Rijeka, Croatia
[2] University of Rijeka, Centre for Micro- and Nanosciences and Technologies, Radmile Matejčić 2, 51000 Rijeka, Croatia

Abstract

Compliant mechanisms gain at least part of their mobility from the deflection of the flexible member. They are characterised by high precision, possibility of monolithic manufacturing, as well as the absence of backlash and wear. Numerical methods are used in this work to characterise the behaviour of compliant rotational mechanisms, known as cross-spring pivots, aimed at ultrahigh-precision positioning applications. The results obtained by using nonlinear finite element calculations are compared with experimental data reported in literature. The finite element model developed in this way makes it possible to conider the influence of lateral loads and of non-symmetrical pivot configurations where the angle or point of intersection of the leaf springs can be varied. This allows assessing the influence of the cited design parameters on the minimisation of the parasitic shifts of the geometric centre of the pivot, as well as on the minimisation of the variability of the rotational stiffness of the pivot while ensuring its stability. The obtained results allow determining design solutions applicable in ultrahigh-precision positioning applications, e.g. in the production or in handling and assembly of MEMS devices.

Keywords: *compliant devices, cross-spring pivots, ultrahigh-precision positioning, FEA modelling, parasitic displacements, rotational stiffness*

1. Introduction

Compliant mechanisms, a viable alternative to sliding and rolling mechanisms used to transfer motion, energy and power, are specific in the sense that they gain at least part of their mobility from the deflection of flexible members. Compliant devices are hence characterised by high precision, the possibility of monolithic manufacturing (thus enabling the adoption of the 'design for no-assembly' approach), reduced costs and the absence of backlash and wear. They are thus widely used in mechanical engineering design, precision engineering as well as the micro- and nanotechnologies [1].

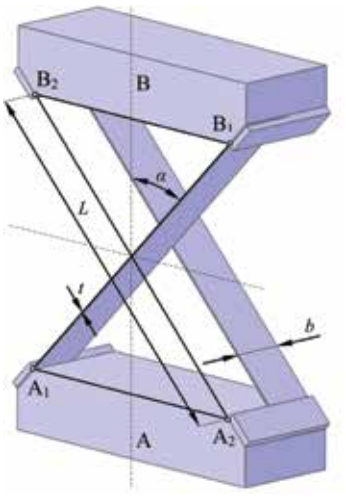

Fig. 1. Typical configuration of a cross-spring pivot

The design of compliant rotational mechanisms known as the cross-spring pivot (Figure 1) is characterised by high compliance along the 'in plane' rotational degree of freedom. Cross-spring pivots are then configured by using two rigid bodies A and B connected via leaf springs which intersect at their midpoint O. The employment of spring-strips enables the prediction of the behaviour of the pivots, which has, however, to be based on the analysis of the characteristic parameters of the strips themselves [1].

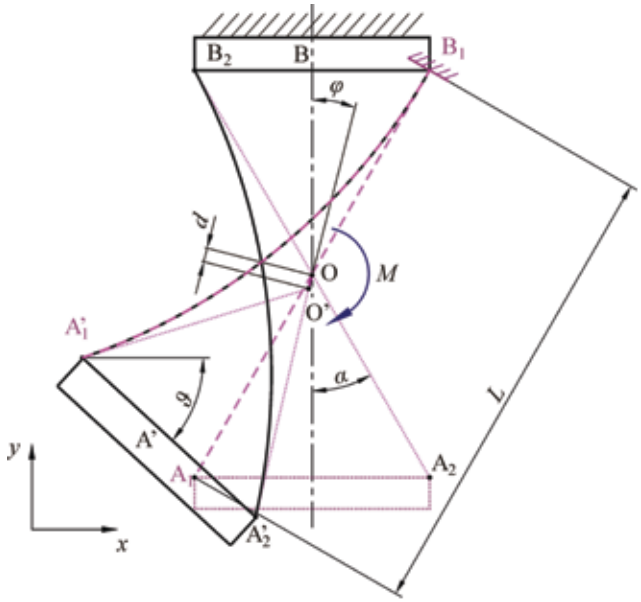

Fig. 2. Analytical model of the cross-spring pivot

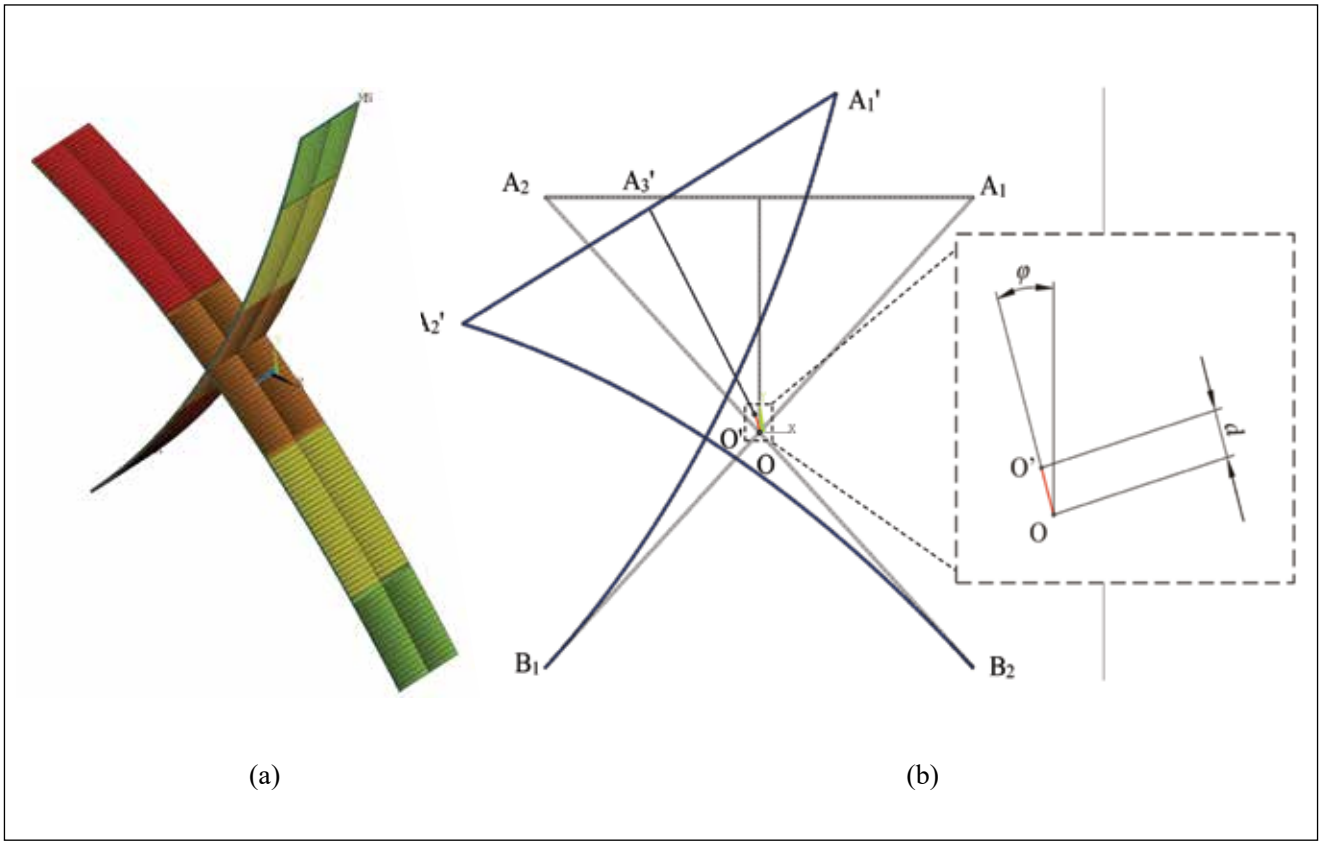

Fig. 3. Meshed FEA model (a) and parasitic motion of the pivot (b)

A typical pivot design configuration, where both leaf springs have the same length L, width b and thickness t, and they are made of the same material, is considered in this work. When loaded with a pure couple M, this configuration allows hence the movable block A to rotate, via the deflection of the leaf springs, with respect to the fixed block B. For larger rotation angles θ, the 'geometrical' centre of the pivot O moves, however, to O', giving rise to a parasitic shift of amplitude d and phase φ that is detrimental to the precision of the analysed mechanisms (Figure 2) [1-3].

By using the finite element analysis (FEA) approach, a numerical model is developed in the ANSYS software environment, enabling to perform nonlinear large deflection analyses of cross-spring pivots in the described loading condition. The considered geometry of the spring-strips in all the subsequent treatise is: L = 115 mm, b = 15 mm and t = 0.5 mm, $2\alpha = 90°$. Line elements (BEAM189), based on Timoshenko beam theory, are used to create the one-dimensional idealization of three-dimensional structure, since such an approach is computationally more efficient with respect to the one where solids and shells are used, while supporting also nonlinear analyses, including the effects of large (geometrically nonlinear) deformations [1]. The mashed model of cross-spring pivot is shown in Figure 3a.

As pointed out, the parameter that determines the rotational accuracy of cross-spring pivot is the parasitic shift of its geometric centre. The x and y components of the parasitic shift can be easily determined from the calculated shift of the free end O of a thin stiff beam attached to the movable block of the pivot as shown in detail in Figure 3b.

The usage of BEAM189 elements implies that the plain strain state is assumed. To enable a high-precision assessment of the parasitic shifts, the anticlastic curvature effect has, however, to be also taken into account. Anticlastic curvature occurs in the leaf springs in the transversal direction (i.e., along their width) and induces stiffening that is nonlinearly proportional to the deflection induced by bending. To duly consider this effect, in the equation of beam curvature the nominal value of Young's modulus E has to be gradually modified towards $E/(1-\nu^2)$, where ν is the Poisson's ratio of the spring-strip material. The dependence of the spring-strip stiffness on its bending has, thus, to be expressed in terms of a modified modulus, defined as [4-5]:

$$E' = \Phi E \tag{1}$$

where Φ, for an instantaneous curvature r of the spring (i.e., its bending curvature), and the herein considered geometrical configuration with the respective ratio b/t = 30, is shown in Figure 4. Values of Young's modulus are thus modified in accordance with Figure 4 and imported in the parameters defining the material model of leaf-springs in the FEA calculations. The resulting analysis showed that the influence of anticlastic curvature is not too large and, for pivot's rotations $\theta \leq 30°$, does not exceed 1 % [1].

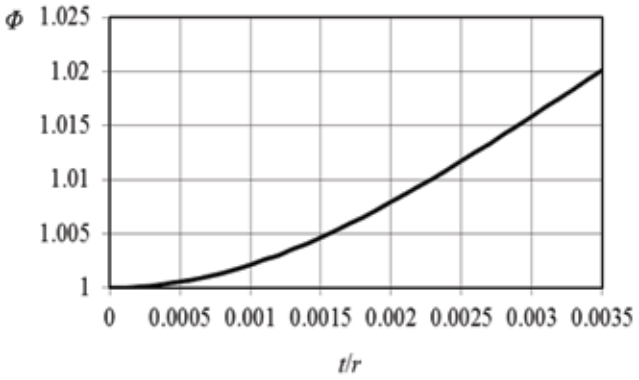

Fig. 3. Change of the transversal stiffness of the leaf springs vs. its instantaneous bending radius r

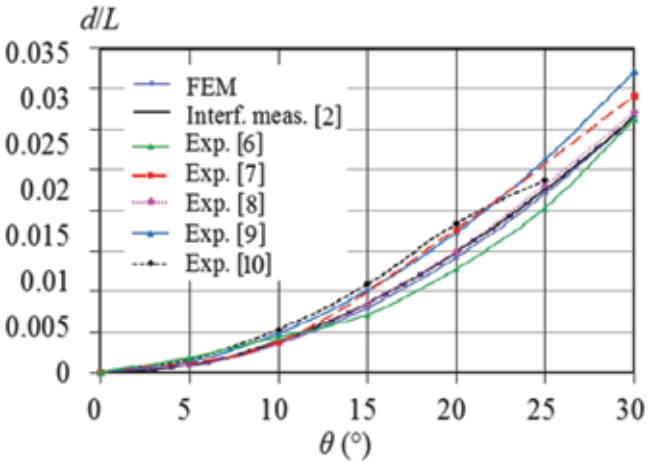

Fig. 5. Comparison of normalized parasitic shift values d/L obtained via experiments and by using the herein developed FEA model

To assess then the applicability of the developed numerical model in predicting the stress-strain behaviour of the considered class of mechanisms, results obtained via the developed FEA model, in terms of the calculated normalized parasitic shift amplitude d/L, are compared with the data of the experimental measurement reported in available literature [2, 6-10]. From the data depicted in Figure 5 it can thus be deduced that the results obtained via FEA are in excellent agreement to those attained via interferometric measurements [2], i.e., conducted by using a high-resolution measurement technology characterised by high accuracies and small intervals of uncertainty. In fact, the difference between these two sets of data is always smaller than 2 % throughout the considered range of rotations of the pivot ($0 < \theta \leq 30°$). The errors inherent in less accurate measurements result, in turn, generally in bigger differences with respect to both the interferometric measurement data and the results of the performed FEA calculations [1]. What is more, FEA results were shown also to be practically coincident to those obtained by a canonical Elastica-type approach of calculation of geometrically nonlinear deflections of spring-strips loaded with torques and forces of various orientations [11].

2. Influence of pivot's design parameters

The above analyses allowed verifying that FEA is suitable for modelling the behaviour of cross-spring pivots. With the goal of minimising the parasitic shifts and the variability of rotational stiffness, while taking into account also the stresses occurring in the pivots, the hence developed FEA model allows considering next alternative design configurations, i.e., varying the design parameters of the pivots. The considered variable design parameters are [1]:

- the angle α and the position of the intersection of the leaf springs (Figure 6),
- a monolithic configuration with the spring-strips joined in point O, and
- the effects of additional external loads of various orientations applied to the pivot.

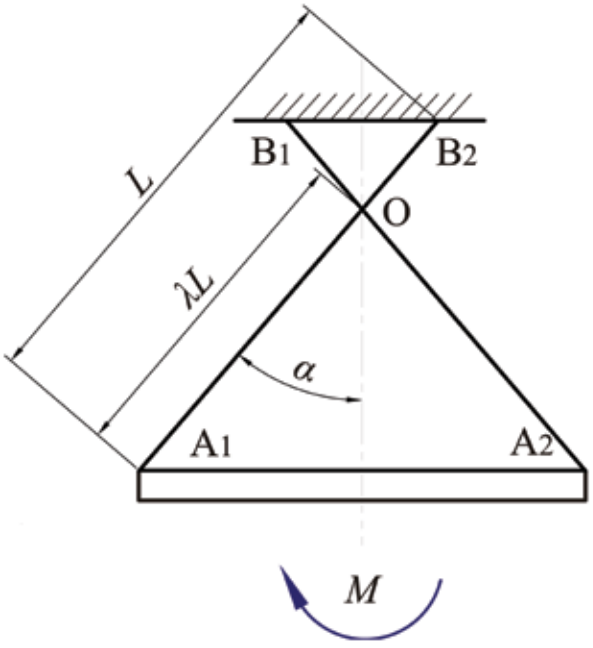

Fig. 6. Non-symmetrical cross-spring pivot configurations

In Figure 7 is hence depicted the influence of a change of the inclination of the leaf springs (i.e., the variation of the angle α) on the normalised parasitic shift amplitudes d/L (Figure 7a), on rotational stiffness $K = M/\theta$ (Figure 7b) and on the maximal stresses σ induced in the fixtures of the leaf springs (Figure 7c). It can be observed that an increase in the value of α and of pivot's rotation θ causes a rise of the values of the normalized parasitic shift amplitudes, an exponential increase of the rotational stiffness and an almost linear increase of the stresses in the clamped ends [1].

(a)

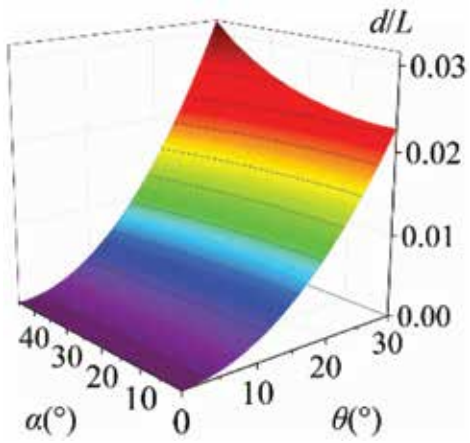

(b)

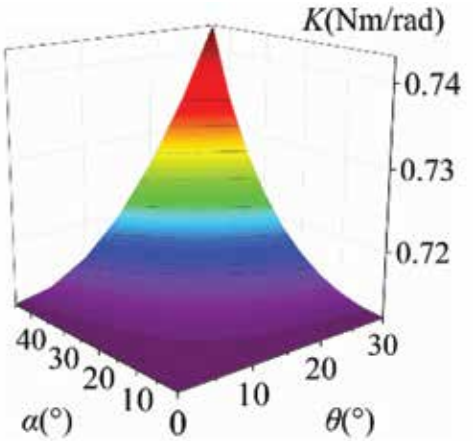

(c)

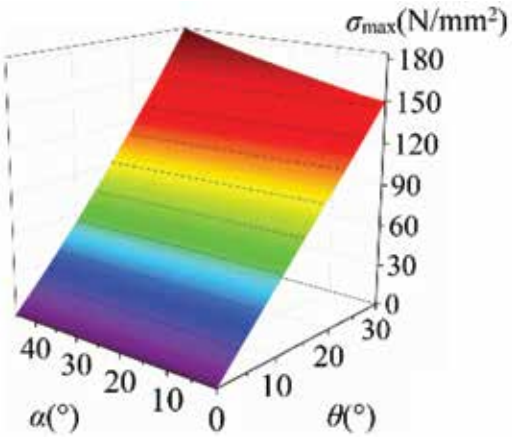

Fig. 7. Change of d/L (a), K (b) and σ (c) depending on the change of the inclination of the leaf springs α and pivot's rotation θ

When, in turn, the position of the geometrical centre of the pivot O, defined with the parameter λ (cf. Figure 6) is analysed, while $\alpha = 45°$, results depicted in Figure 8 are obtained. The thus induced variations of the normalised parasitic shift amplitudes d/L (Figure 8a), of the rotational stiffness K (Figure 8b) and of the stresses σ in the fixtures (Figure 8c), are again considered.

(a)

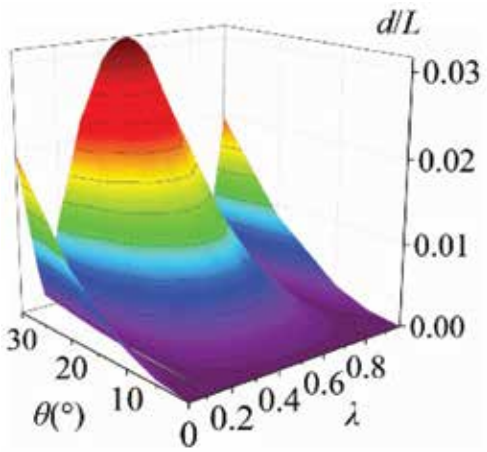

(b)

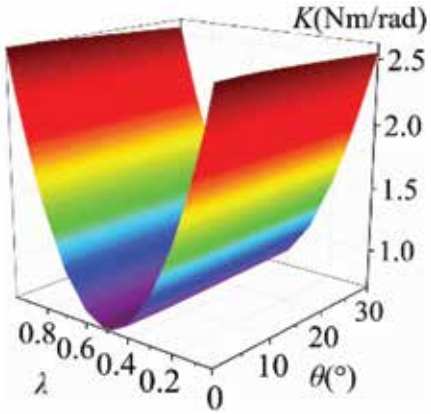

(c)

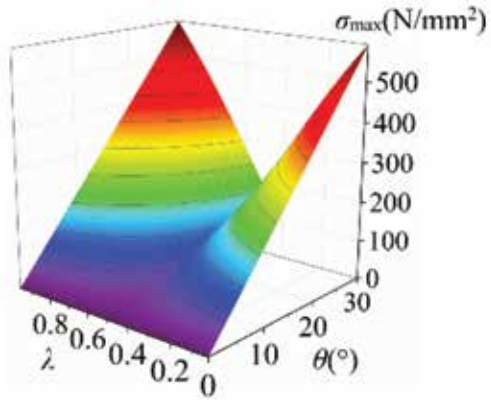

Fig. 8. Change of d/L (a), K (b) and σ (c) depending on the change of the position of the intersection of the springs λ and pivot's rotation θ

It can thus be concluded that a change of λ causes a substantial nonlinear variation of all the resulting parameters defining the behaviour of the cross-spring pivots. It is very important to note here, however, that, even for large pivot rotations θ, a design configuration for which $\lambda \approx 0.13$, results in negligible parasitic shift amplitudes, although at the expense of a large increase of rotational stiffness as well as of the stresses. Contrary to what is generally reported in literature, the performed nonlinear FEA calculations also allow the conclusion that the λ value for which d/L is minimised is not constant, but changes depending on the value of α in the range $0.127 \leq \lambda \leq 0.175$ [1].

When the monolithic configuration of the cross-spring pivot, with the spring-strips joined in their midpoints, is considered (Figure 9), results shown in Figure 10 are obtained. It is clear that in this case values of the normalised parasitic shift amplitudes d/L of up to about 10 times lower with respect to the previous cases are attained. This is achieved, however, at the expense of a 5-fold increases of the stiffness and of a 4-fold increase of the stresses with respect to the conventional cross-spring pivot configuration of Figure 1.

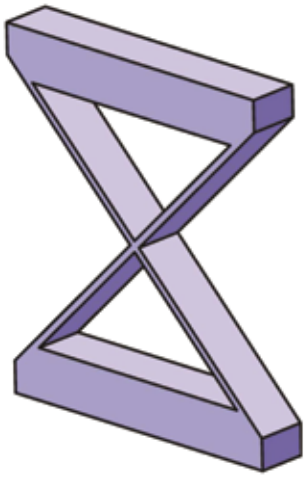

Fig. 9. Monolithic cross-spring configuration

(a)

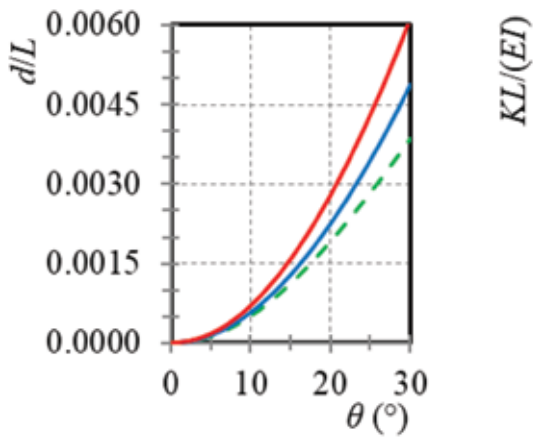

(b)

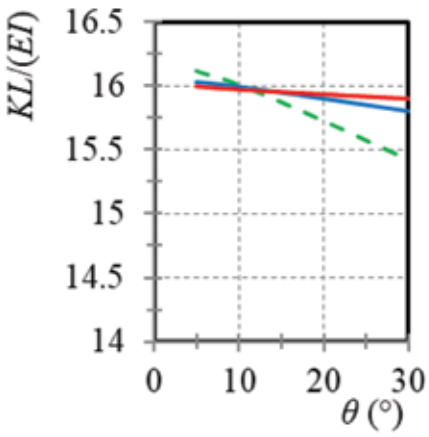

(c)

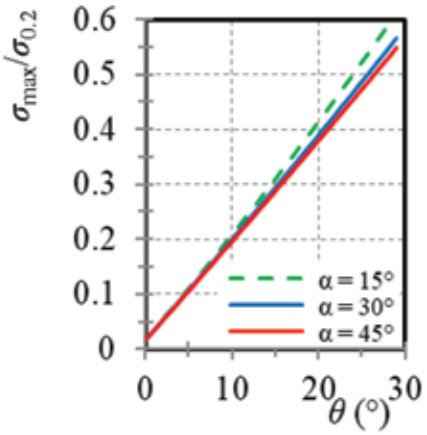

Fig. 10. Change of d/L (a), K (b) and σ (c) for the monolithic cross-spring pivot configuration depending on pivot's rotation θ for various α values

In [1] a composite pivot design configuration of Figure 11 is also considered. Although it allows diminishing even further the parasitic shifts with lower stress levels than in the monolithic pivot configuration, this configuration is certainly very complex from the technological point of view, so that its applicability is questionable.

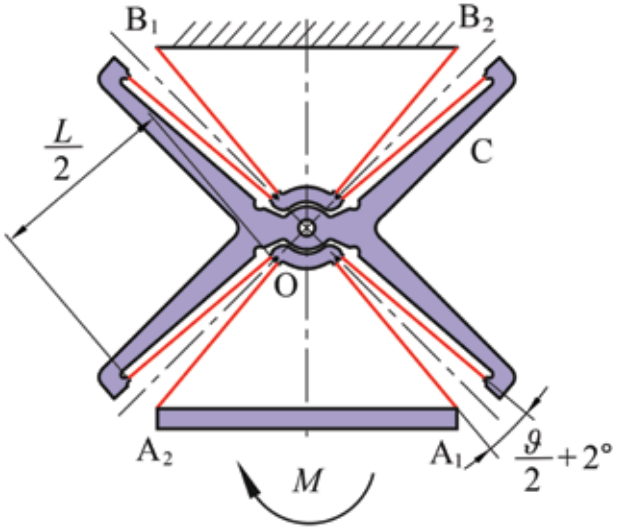

Fig. 11. Composite cross-spring pivot design configuration

The analysis of the influence of external loads on the variability of rotational stiffness and on the value of the parasitic shifts is finally performed [1]. The pivot is hence loaded as shown on Figure 12.

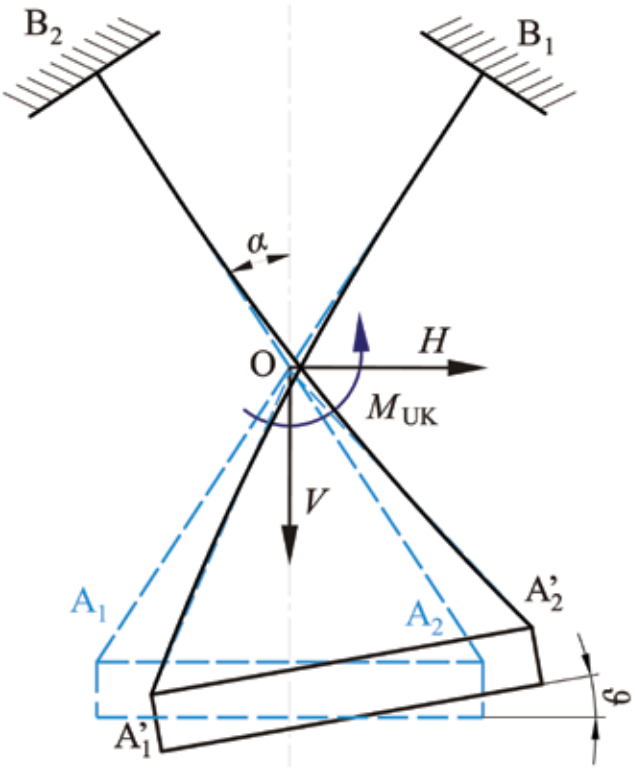

Fig. 12. Pivot loaded with external loads

Physically, the horizontal force H and the torque M superimpose, so the influence of H is taken into account as a contribution to M. The results of numerical analyses of the influence of the vertical force V loading the pivot, along with M, on rotational stiffness allow then evidencing that a compressive vertical force V_C narrows the stability range of the pivot (that where its rotational stiffness is positive), induces an increase of rotational stiffness but also a decrease of the parasitic shifts. On the other hand, the action of a tensile vertical load V_T results in a decrease of the rotational stiffness and an increase of parasitic shifts. When a variation λ is considered as well, V_T results, in turn, in widening the stability range (Figure 13a). A design configuration with $\lambda = 0.1$ allows thus attaining a very stable value of the rotational stiffness and, concurrently, small parasitic shifts, in the whole range where $V_TL^2/(EI)$ is smaller than 30 (Figure 13b), whereas the configuration with $\lambda \approx 0.13$ results in a stable rotational stiffness value in the range where $|VL^2/(EI)| \leq 10$ regardless of the vertical load orientation (Figure 13c) [1].

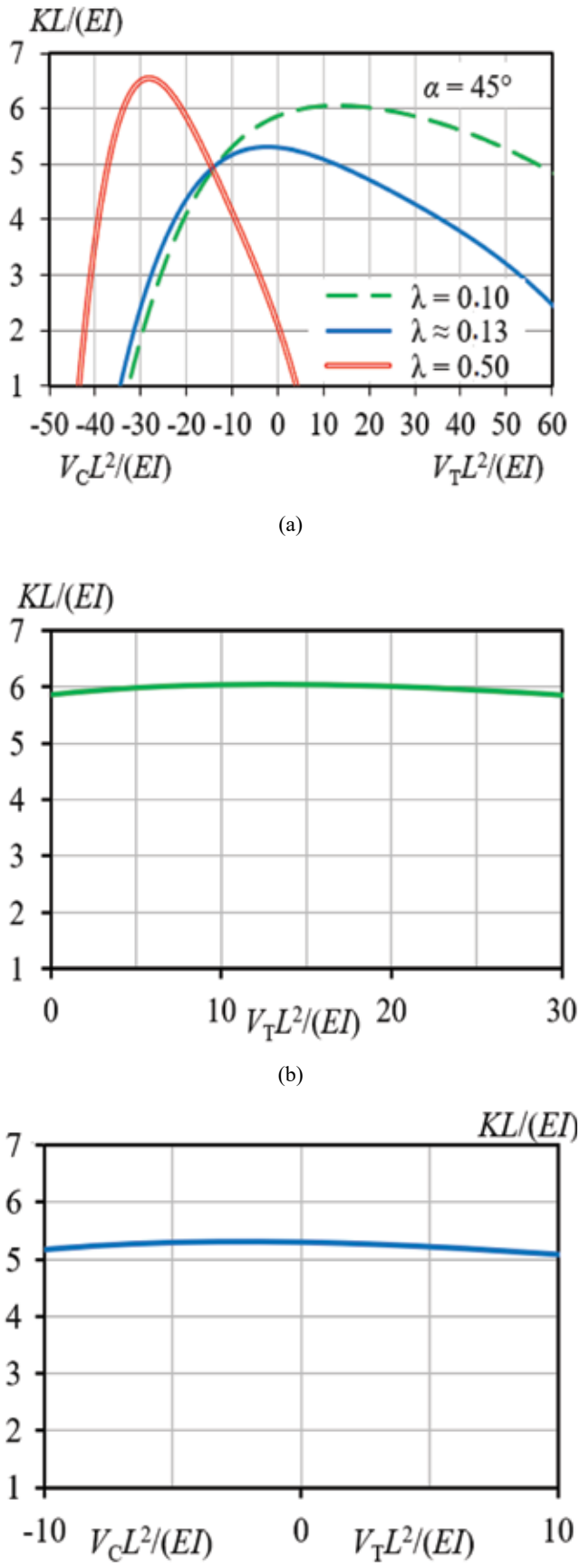

Fig. 13. Rotational stiffness dependence on vertical loads (a) minimized variation of rotational stiffness for $\lambda = 0.1$ (b) and $\lambda \approx 0.13$ (c)

3. Conclusions

The comparison of the results on the behaviour of cross-spring pivots aimed at ultrahigh-precision positioning applications obtained via the developed nonlinear FEA models to experimental data, performed in this work, allows confirming the validity of the FEA models even when large pivot rotations, inducing geometrical nonlinearities, are to be considered. Nonlinear FEA is hence used to attain quick, accurate and reliable results in thoroughly studying the influence of various pivots' geometric and loading conditions on the possibility to minimize the parasitic shifts and the variability of the stiffness of the pivots. Thus it could be established that an optimal design configuration will always be based on a compromise between configurations that allow improving some characteristic parameters of the pivots, while deteriorating, at least partially, some of the others.

A technologically easily achievable cross-spring pivot design with the value of the geometric parameter $\lambda \approx 0.13$ allows, then, attaining ultrahigh-precisions, as it is characterized by negligible parasitic shifts even for large pivot rotations, while concurrently guaranteeing the stability of the mechanism and the maintenance of the stress levels well within the allowable limits. The values of λ that allow minimising parasitic shifts depend, however, on spring-strips' inclination α, on the range of rotations θ, as well as on the external forces loading the pivot. A pivot design with $\lambda \approx 0.13$ and $\alpha = 45°$ is characterized by small parasitic shifts, but also by very limited variations of rotational stiffness. On the other hand, pivot configurations with $\lambda = 0.1$ allow achieving small rotational stiffness variations and small parasitic shifts for a rather large span of tensile vertical loads.

Simple and reliable cross-spring pivot design configurations with the values of the geometric parameter in the $0.1 \leq \lambda \leq 0.13$ range could, therefore, be applied in a broad range of ultrahigh-precision micropositioning applications such as, for instance, in the field of the production or of handling and assembly of micro-electromechanical systems (MEMS).

References

[1] Marković, K. and Zelenika, S. (2017). Optimised cross-spring pivot configurations with minimised parasitic shifts and stiffness variations investigated via nonlinear FEA. *Mechanics Based Design of Structures and Machines* 45*(3)* 380-94.

[2] Zelenika, S. and De Bona, F. (2002). Analytical and experimental characterisation of high-precision flexural pivots subjected to lateral loads. *Precision Engineering* 26 381-8.

[3] Haringx, J. A. (1949). The Cross-Spring Pivot as a Constructional Element. *Applied Scientific Research* A1*(4)* 313-32.

[4] Ashwell, D. G. (1950). The anticlastic curvature of rectangular beams and plates. *Journal of Royal Aeronautical Society* 708-15.

[5] Angeli, P., De Bona, F. and Munteanu, M. Gh. (2006). Micromeccanismi con molle a lamina: valutazione della rigidezza flessionale. In *Proceedings of the 35th AIAS National convention* Ancona (IT).

[6] Siddall, G. J. (1970). The Design and Performance of Flexure Pivots for Instruments. M. Sc. Thesis, University of Aberdeen, UK.

[7] Young, W. E. (1944). An Investigation of the Cross-Spring Pivot. *ASME Journal of Applied Mechanics* 11 A113-20.

[8] Wuest, W. (1950). Blattfedergelenke für Messgeräte. *Feinwerktechnik* 54*(7)* 167-70.

[9] Nickols, L.W. and Wunsch, H. L. (1951). Design Characteristics of Cross-Spring Pivots. *Engineering* 473-76.

[10] Hildebrand, S. (1958). Obliczanie i zachowanie sie w pracy sprezyn krzyzowych. *Pomiary-Automatyka-Kontrola* 11 501-8.

[11] De Bona, F. and Zelenika, S. (1997). A generalized Elastica-type approach to the analysis of large displacements of spring-strips. *Proceedings of the Institution of Mechanical Engineers, Part C: Journal of Mechanical Engineering Science* 211*(7)* 509-17.

Petar Gljušćić[1, 2] *and Saša Zelenika,*[1, 2]

Energy harvesting for wearable applications

[1] University of Rijeka, Faculty of Engineering, Vukovarska 58, 51000 Rijeka, Croatia
[2] University of Rijeka, Centre for Micro- and Nanosciences and Technologies, Radmile Matejčić 2, 51000 Rijeka, Croatia

Abstract

Energy harvesting, the process of collecting low level ambient energy and converting it into electrical energy, is a promising approach to power wearable devices. By converting the energy of the human body by using piezoelectric and thermoelectric principles, the need for batteries and charging can be avoided, and the autonomy of wearable devices can be significantly increased. Due to the inherent random nature of human motion, however, the energy harvesting devices need to be specifically designed in order to ensure their optimal operation and sufficient power generation. Using several combined approaches, a new class of autonomous devices, suitable for telemedicine, patient monitoring or IoT applications, can be developed.

Keywords: *wearable technologies, energy harvesting, broadband piezoelectric devices, geometry optimization, frequency up-conversion, thermoelectric energy harvesting*

1. Introduction

Energy harvesting (EH) - the process of collecting low-level ambient energy and its conversion into electrical energy, is an increasingly studied approach to reduce or eliminate battery usage in various devices, resulting in the potential development of novel autonomous systems. The generally considered forms of available ambient energy are kinetic (vibrations), thermal (waste heat), solar and radio frequency (RF) sources. An ubiquitous energy source is certainly kinetic energy, present in all moving systems, which can thus be collected and converted into electrical energy by using various technologies, the most common being piezoelectric and electromagnetic transducers [1-2]. The generally used form of piezoelectric transducers are bimorph cantilevers, in the design configuration shown in Figure 1, comprising two piezoelectric layers on a metallic substrate, clamped at the end subject to external dynamical excitations. The tip mass on the free end serves, in turn, as a deflection amplifier and for tuning the response of the device to a specific excitation frequency [3].

2. Wearable technologies

The term wearable technologies (or wearables) usually encompasses a range of devices, generally sensors, with data acquisition, processing and transmission components (Figure 2) [3], that can be worn as a typical accessory (e.g. a wrist watch, smartphone or as part of clothing), and used for a variety of purposes, from health monitors (blood pressure, heart rate, blood glucose levels), to automated drug (e.g. insulin) delivery systems.

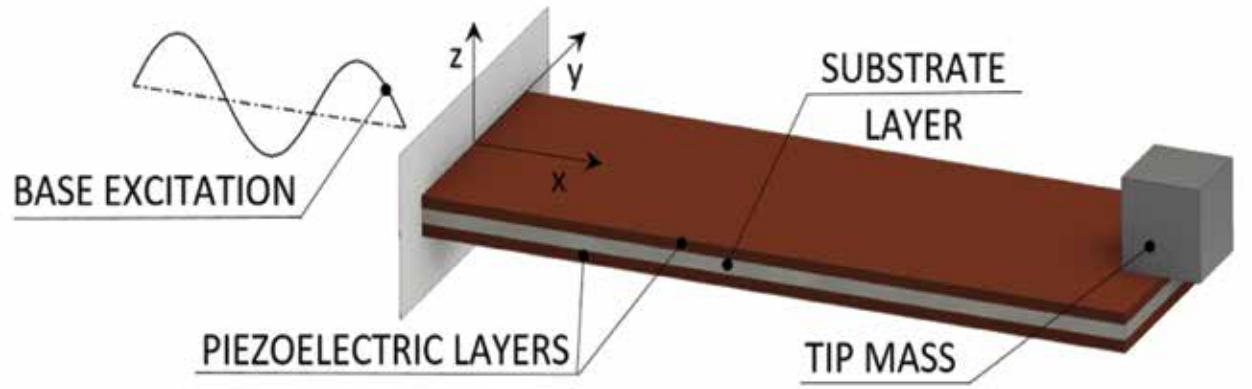

Fig. 1. Bimorph piezoelectric energy harvester [3]

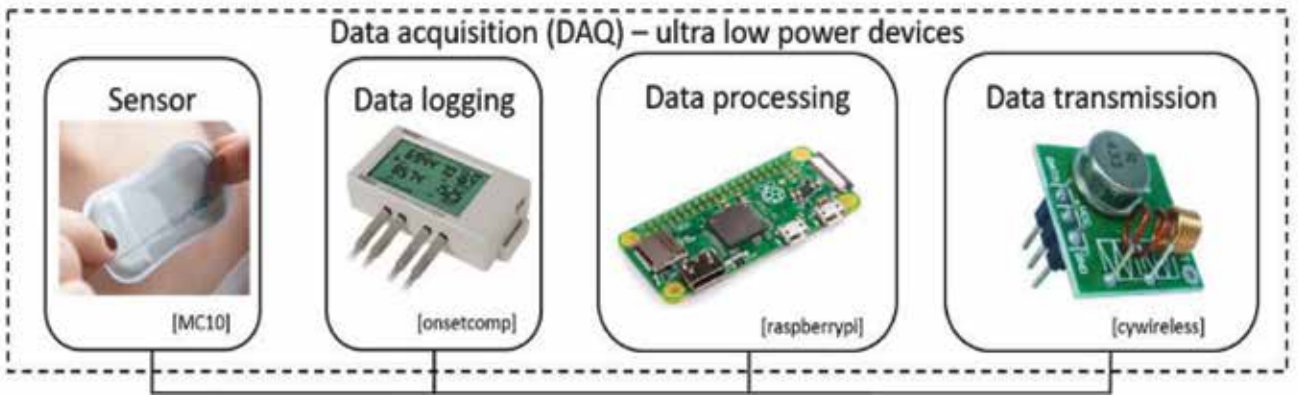

Fig. 2. Components of a typical wearable system

As all electronic devices, in order to operate, wearables require electrical energy, usually supplied by a battery, which needs to be replaced or recharged, causing a negative environmental impact and reducing the autonomy of the devices – which is especially important in telemedicine, when wearables are used in remote patient monitoring. The power requirements of typical wearable device components have been thoroughly analysed in literature, allowing to conclude that the sensors generally require relatively low power levels (from tens of μW up to a couple of mW), while other components, including data processing and transmission components, can often necessitate larger power levels [3-4]. This issue can be resolved by reducing the active time of such components, e.g. by minimizing the data transfer intervals, according to appropriate medical practices [3].

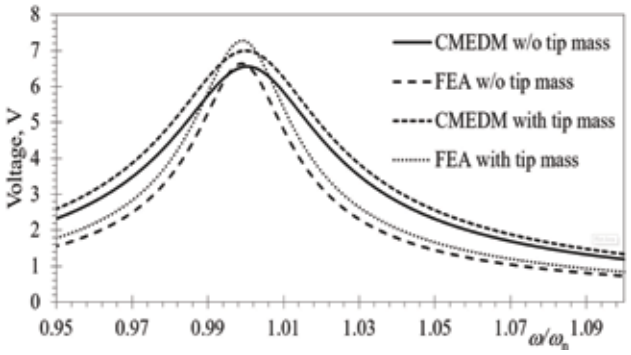

Fig. 3. Electromechanical response of a rectangular bimorph PEH [3]

On the other hand, the human body produces significant amounts of energy, the most promising being the energy of human motion, e.g. arm movement or walking/running, with available power levels up to ~ 60 W [5]. A conventional power source for wearables can, thus, be replaced by an EH system positioned on the body, such as the described piezoelectric energy harvester (PEH), hence enabling a novel class of autonomous wearable devices that do not require battery recharging or replacement.

3. Issues with PEHs in wearable technologies

A major issue inherent to bimorph PEHs is their narrow area of optimal operation around the eigenfrequency of a specific device (Figure 3), with a significant drop in output voltages and powers as soon as the base excitation drifts away from the eigenfrequency [3].

This issue is particularly evident when PEHs are employed in wearable technologies. In fact, the excitation generated by human motion results in random vibrations. Figure 4 shows thus the EH voltage output for devices excited by random human motion such as walking, measured in the wrist and head areas [6]. In such cases it is difficult or even impossible to properly tune the PEH to ensure its optimal operation.

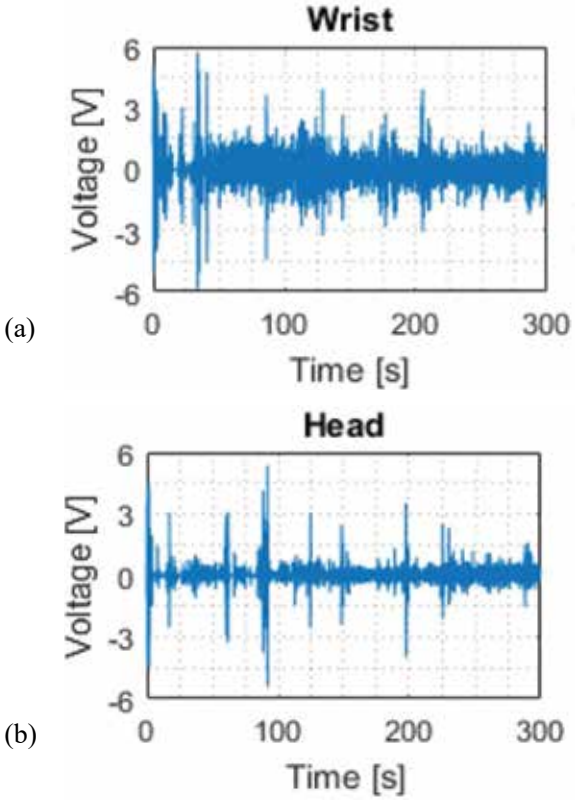

Fig. 4. Examples of random human motion excitations by walking measured in the wrist (a) and head (b) areas [6]

Several methods of widening the optimal spectrum of PEH operation, and thus overcome the above described issue, have been proposed in literature. Those considered as the most promising ones are [3, 7]:

- changing the conditions around the free end of the PEH (e.g. via active tuning or damping control);
- changing the cantilever geometry (e.g. by using several differently tuned PEHs, via complex geometries or by resorting to bi-stabile nonlinear responses);
- frequency up-conversion (FUC) mechanisms (i.e., by plucking the PEH's free end and letting it oscillate at its eigenfrequency).

The focus of our work is to analyse the influence of the geometry on PEH's response, and to find a way to combine a geometry change approach with a FUC mechanism, so as to achieve optimal operation even with random excitations generated by human movements.

To be able to accurately simulate the behaviour of the resulting devices, a suitable model is needed. Although several mathematical models that describe the PEH response do exist, the most accurate was proven to be the recently developed "coupled modal electromechanical distributed parameter model" (CMEDM) [8]. Although this model allows overcoming many disadvantages of prior models, it is still limited to a cantilever with a constant rectangular cross-section. In order to analyse the effects of a geometry variation on PEHs' response, a more flexible yet complex finite element (FE) numerical model is thus developed using ANSYS® [3]. The FE model comprises three separate analyses:

- **modal analysis:** determination of the mechanical dynamical response and the respective eigenfrequencies;
- **coupled harmonic analysis:** determination of the coupled electromechanical dynamical responses;
- **coupled transient analysis:** linear and nonlinear (including geometrical nonlinearities) determination of dynamical responses under forced excitation in discrete time steps.

3.1. Modal analysis

The initial step of the FE modelling process is the modal analysis, validated by comparison with CMEDM. This step is needed to determine the eigenfrequencies of the PEH. In the herein considered case, only the first modal shape is considered, since the largest deflections, and hence the highest output voltages, are achieved in this state. Within this step only the purely mechanical response of the PEH is observed, while the piezoelectric properties of the material are set to zero. The performed mesh sensitivity analysis allowed then concluding that it has a negligible influence on the calculated eigenfrequency. A coarser mesh can thus be used in the subsequent FE analyses, reducing the required processing power requirements and analysis times [3].

3.2. Coupled harmonic analysis

After the initial modal analysis, several coupled harmonic analyses are performed in order to determine the coupled dynamical electromechanical responses (coupled FRFs) of the considered PEH. The harmonic excitation bandwidth of the fixture is thus set around the eigenfrequency value determined via the modal analysis, while the other boundary conditions remain unchanged. In order to simulate a resistive load, enable output voltage estimation, and calculate PEH's output power, a variable resistor element is then introduced into the model between the charge collecting points [3].

A major requirement needed to obtain accurate results of harmonic analyses is the definition of damping. Rayleigh damping, commonly used in FE analyses, is therefore calculated based on the experimentally attained damping coefficients ζ. By performing several harmonic analyses while varying the excitation frequencies and the attached load resistances (from the Ω up to the MΩ range), coupled harmonic responses are obtained, allowing to determine the optimal resistance value, i.e., that where the highest output voltage is achieved [3].

3.3. Coupled transient analysis

Linear and nonlinear coupled transient analyses are performed next to attain the dynamical responses of the PEH subjected to forced excitation in precisely defined discrete time increments. A sinusoidal excitation profile is hence introduced and applied to the clamped base, while the PEH geometry and the boundary conditions remain identical to those in the harmonic analysis. With the occurrence of large deflections, nonlinear effects become more relevant, so that the responses can no longer be predicted by the assumptions of the linearized Euler-Bernoulli model, and a nonlinear transient analysis has to be used (Figure 5) [3].

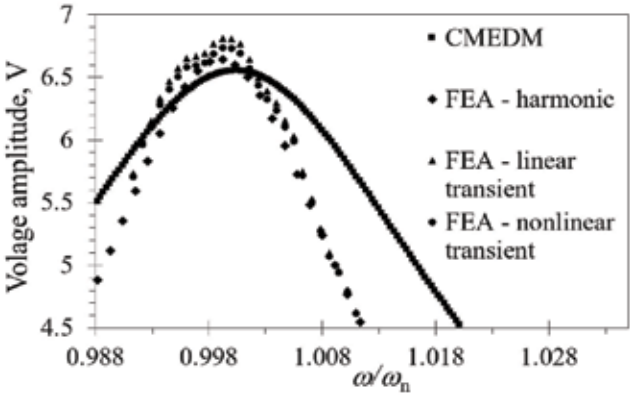

Fig. 5. Linear and nonlinear FEA transient responses for a rectangular PEH [3]

4. Influence of geometry on PEH response

By means of FE analyses as well as experimental measurements, it has recently been demonstrated that by changing the geometry of a conventional rectangular PEH to an optimized trapezoidal shape, the specific power output of the considered EH device can be significantly increased. A further increase was then achieved by clamping the trapezoidal PEH at its narrow end, i.e., when an inverse trapezoidal shape is used [9].

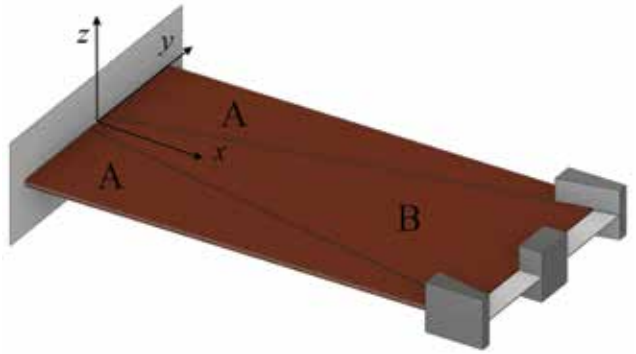

Fig. 6. Segmented PEH geometry [10]

Due to a limited available volume (i.e., limited PEH surface area) inherent to wearable devices, a conventional rectangular PEH shape (indicated with R) of a predefined surface area can thus be segmented, as shown in Figure 6. Two trapezoidal (A) and one inverse trapezoidal shape (B) are thus attained, potentially resulting in an increase of the specific power outputs, while keeping the surface area (and volume) unchanged. The respective voltage and power output values are hence calculated by performing several FE analyses for each segment of the resulting design configuration, while varying the respective load resistances. The obtained specific power output values, normalized w.r.t. the surface areas, are depicted in Figure 7, where a significant specific power increase of the segmented PEHs can be observed [3, 10].

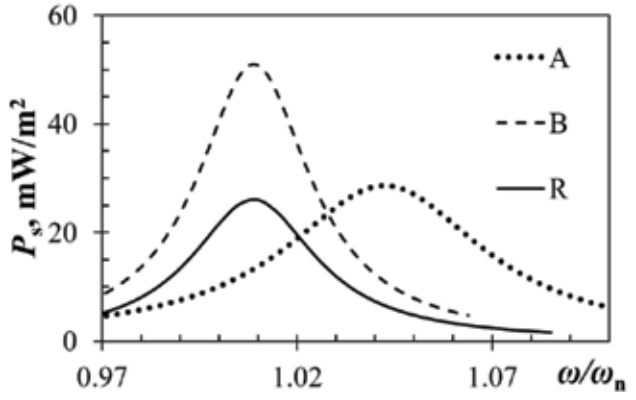

Fig. 7. Comparison of specific power outputs of rectangular and segmented PEHs [10]

The power output of PEHs can be further increased by introducing various stress concentrators in the form of notches and waves into the geometries. Two different approaches are being studied in this frame, one with a V-notch at the base of a rectangular PEH (indicated now in Figure 8 as, respectively, design configurations A and B), while the other one comprises a wavy edge on a segmented PEH (indicated as designs C and D). [11].

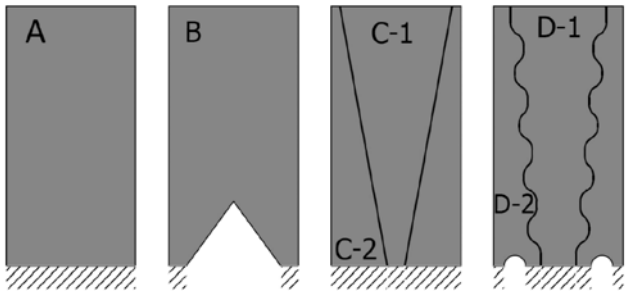

Fig. 8. Increasing PEH power output by introducing stress concentrators [11]

Multiple FE analyses with the attainment of an optimal resistance value for each variant of the PEH design are performed, allowing the output voltages and the respective specific power outputs to be calculated. A noticeable increase in specific powers is thus obtained for the shapes where stress concentrators are introduced (Figure 9) [11].

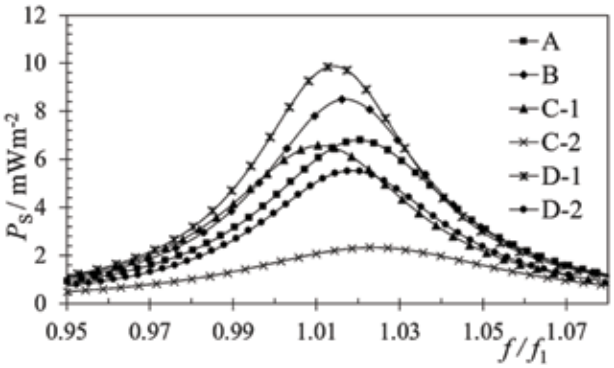

Fig. 9. Specific power outputs for PEHs with added stress concentrators [11]

5. Frequency up-conversion mechanisms

Frequency up-conversion mechanisms are aimed at converting random ambient excitations into a periodic excitation of the PEH. This is achieved by plucking or impacting the cantilever free end and letting the device oscillate at its eigenfrequency. Such configurations thus operate always in optimal conditions, hence overcoming the previously evidenced drawbacks. This approach, combined with a flywheel that converts random kinetic energy from human movements into rotational motion, results then in a system suitable for a wrist watch-like device (Figure 10). The flywheel has a plectrum attached to it and, while rotating, plucks the free end of the PEH.

Such devices, being developed in collaboration with medical institutions, can then comprise one or multiple segmented PEHs, reducing the volume required for power generation, increasing power outputs and, thus, the autonomy of the device [11].

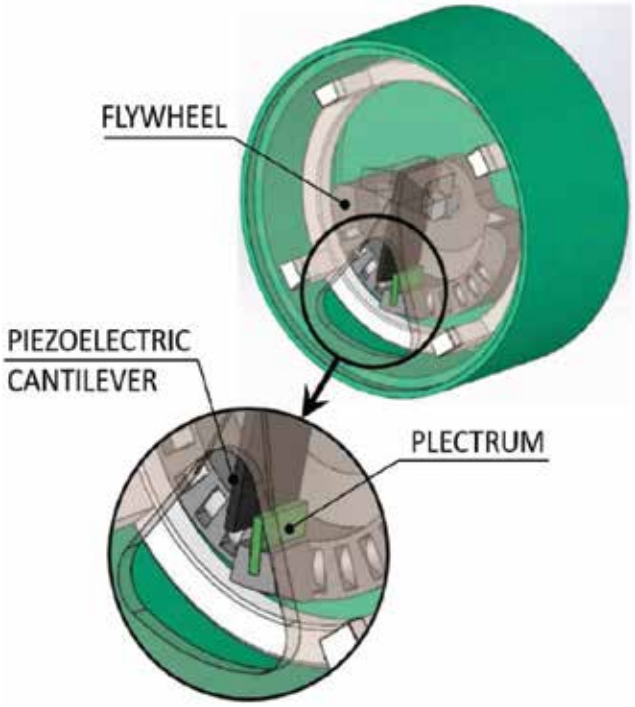

Fig. 10. Wearable watch-like device using a FUC principle [11]

Various effects on the response of a plucked PEH are being evaluated in an ongoing experiment. The studied parameters include the speed and direction of plectrum rotation, i.e., the velocity and direction of the approaching plectrum, as well as the influence of the material properties of the plectrum itself on the PEH response. The respective experimental setup, shown in Figure 11, comprises thus an adjustable clamping base, suitable for the analysis of different PEH sizes, as well as a controllable electric motor with an attached plectrum holder, allowing a quick change of different plectra [11].

A preliminary electromechanical response of a plucked PEH is shown in Figure 12, where the initial cantilever deflection due to the plucking of the free end, as well as the free oscillation of the PEH, can be well observed.

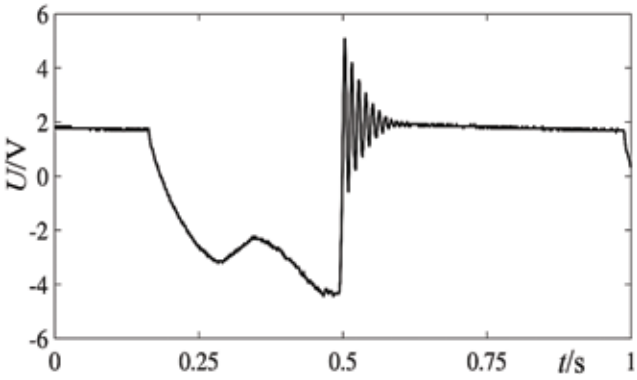

Fig. 12. Electromechanical response of a plucked PEH [11]

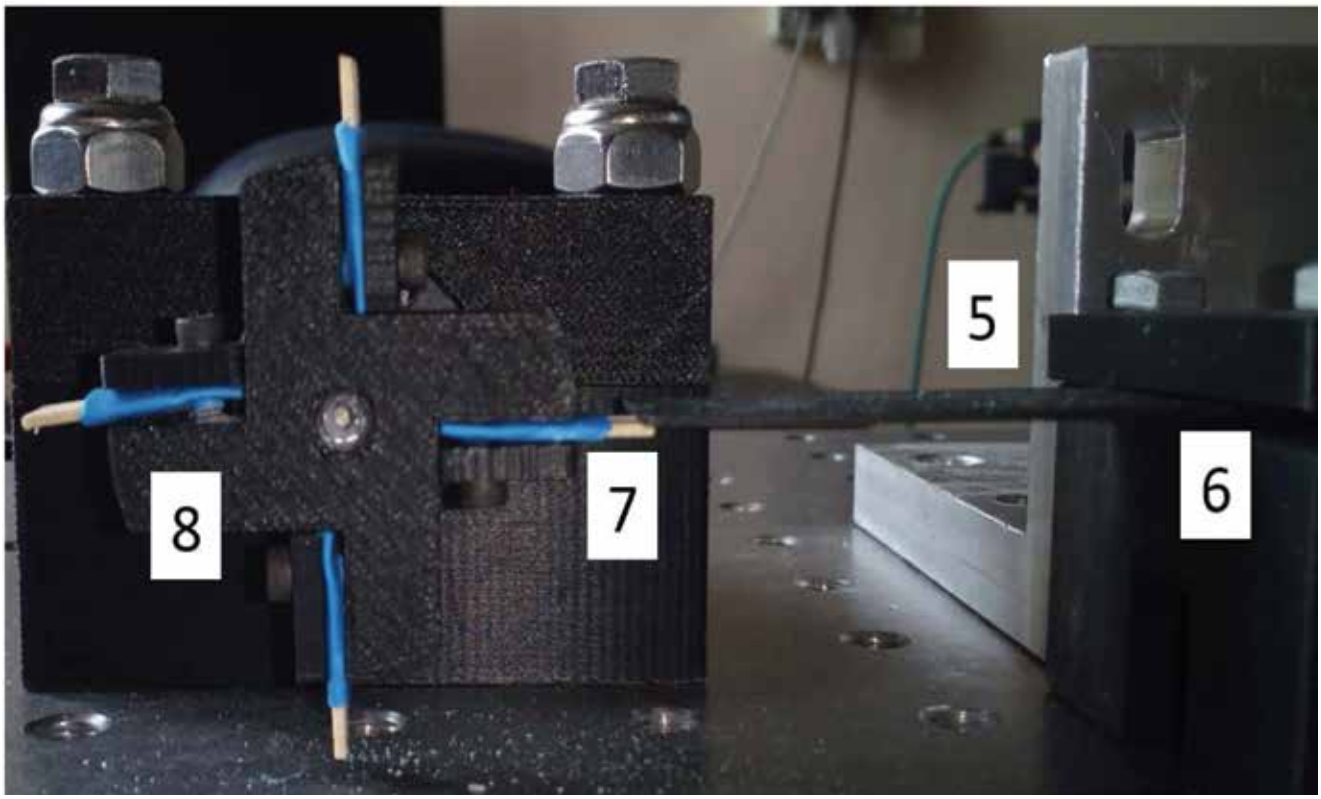

Fig. 11. Frequency up-conversion experimental setup [11]

6. Thermoelectric energy harvesting

Another form of ambient energy available on the human body is waste heat, emitted due to metabolism. Such energy form, i.e., the temperature gradient between the surface of the skin and the surrounding air, can be converted into electrical energy by using a solid state device based on the Seebeck effect, referred to as the thermoelectric generator (TEG - Figure 13) [12].

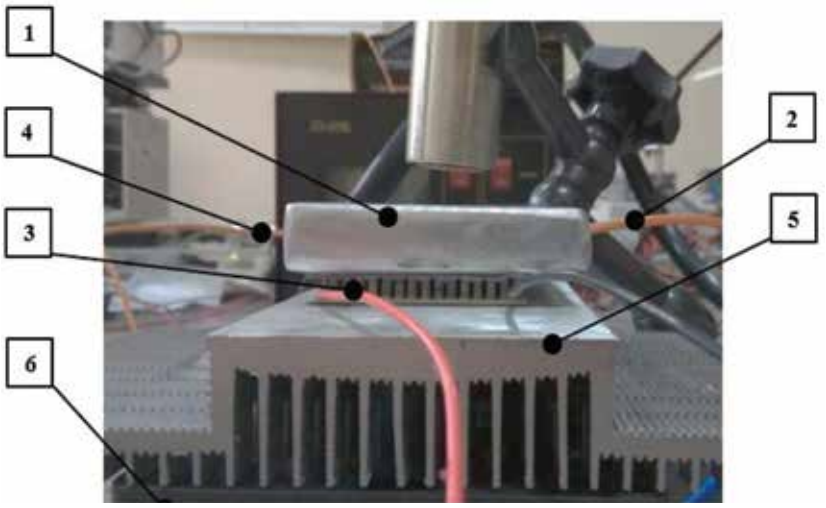

(a)

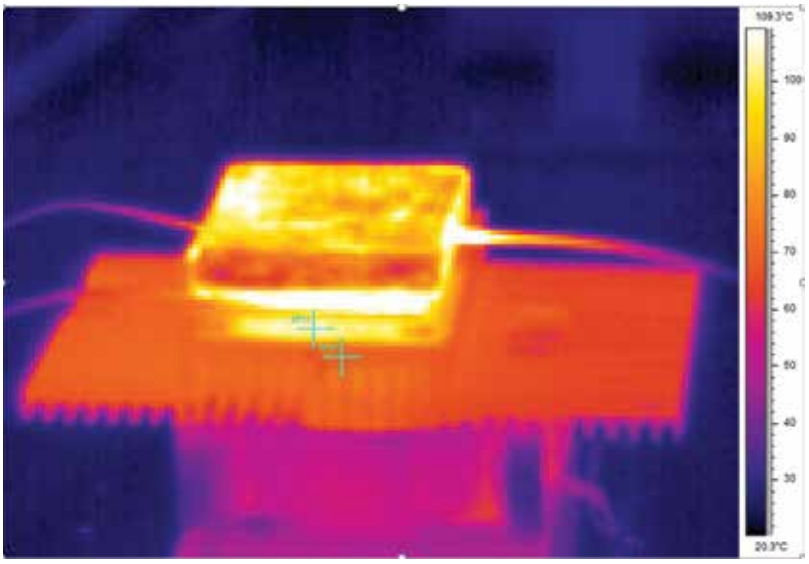

(b)

Fig. 13. TEG as part of an experiment (a), and respective thermal imaging (b) [12]

The main issue with TEGs is their low energy conversion efficiency that decreases with reduced temperature differences. This drawback is, however, at least partially compensated by the simplicity of this type of EH devices, having no moving parts. TEGs can enable also a simple and effective addition to an existing EH system, thus creating a novel hybrid system with extended autonomy, suitable for utilization in wearable technologies.

7. Power management in wearable EH systems

When multiple or segmented PEHs are used, or when different EH devices (e.g. PEGs and TEGs) are concurrently employed, thus creating a hybrid EH system, a suitable power management scheme is needed. In fact, the energy harvested by such systems needs to be properly managed to obtain a smooth and stabilized voltage supply that can be used to power the considered load (various sensors as well as data processing and communication components) [3].

In cases when an energy surplus is produced by the EH system, the task of the hence employed circuitry is also to manage this surplus and store it using a storage element such as a supercapacitor or a rechargeable battery, so that it can be used when it is needed by the wearable device components. The introduction of a storage element allows for short power bursts, which could be useful in time periods when a higher amount of power is needed, e.g. for data transmission [3].

An example of a power management scheme, aimed at managing multiple power inputs as well as to store surplus energy for later use, is shown in Figure 14. The central component of the power management electronics is a DC-to-DC buck converter that enables the collection of low-level energy onto a storage device (capacitor) on the primary side, and transferring it to the secondary side when the levels are high enough to power the wearable components or to charge the main storage element [3].

8. Conclusions and outlook

Energy harvesting is a viable approach to power wearable devices by using energy from the human body in the form of kinetic energy of human motion and/or emitted body heat. Innovative solutions, such as the segmentation of PEH geometry and frequency up-conversion mechanisms, especially when combined, are a promising method of overcoming the inherent drawback of such devices due to the random

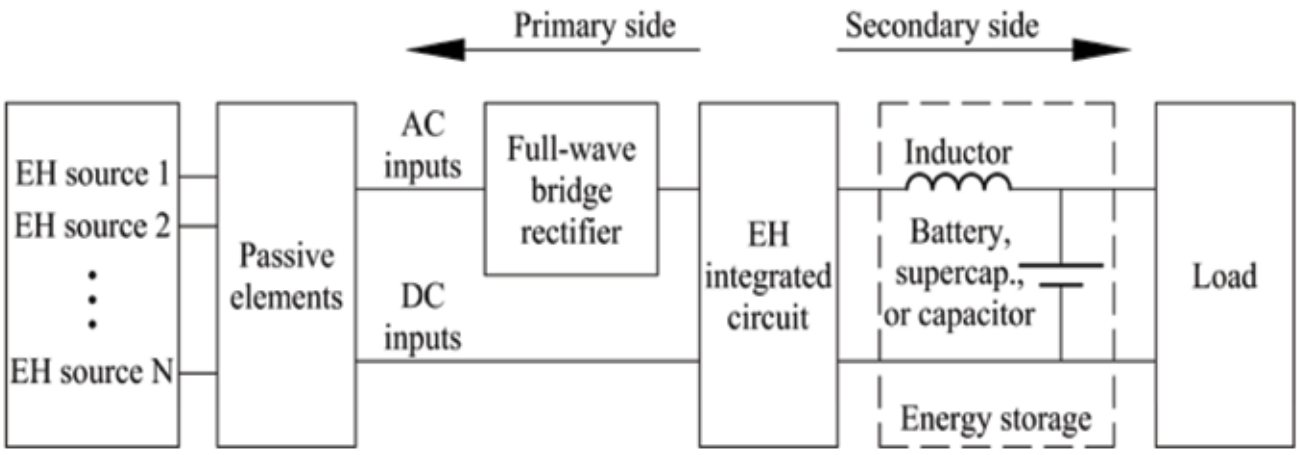

Fig. 14. Wearable EH power management scheme [3]

nature of human motion, particularly evident in wearable applications.

Frequency up-conversion experiments are currently being performed to determine the optimal parameters of the plucking mechanism, i.e., rotational speed as well as the material and number of plectra. Further experimental research is needed to validate the used numerical models, thus perfecting a comprehensive tool for the development of optimized wearable piezoelectric energy harvesting systems.

Thermoelectric energy harvesting technology can then be easily added to a wearable PEH system, making additional electrical energy available, thus forming an innovative hybrid EH system. Such a system can then be used to develop new autonomous wearable devices, suitable to be used in telemedicine, patient monitoring, automated drug delivery and various IoT applications.

Acknowledgements

This work is partly enabled by using the equipment funded via the EU European Regional Development Fund project no. RC.2.2.06-0001: "Research Infrastructure for Campus-based Laboratories at the University of Rijeka (RISK)" and supported by the University of Rijeka, Croatia, project uniri-tehnic-18-32 „Advanced mechatronics devices for smart technological solutions".

References

[1] Kazmierski, T. J. and Beeby, S. (2011). *Energy Harvesting Systems: Principles Modeling and Applications* (Kaizmierski, T. J. ed.), Springer, New York (NY, USA).

[2] Priya, S. and Inman, D. J. (eds.) (2009). *Energy Harvesting Technologies.* Springer, New York (NY, USA).

[3] Gljušćić, P., Zelenika, S., Blažević, D. and Kamenar, E. (2019). Kinetic Energy Harvesting for Wearable Medical Sensors. *Sensors* 19*(22)* 4922.

[4] Oletic, D. and Bilas, V. (2018). System-Level Power Consumption Analysis of the Wearable Asthmatic Wheeze Quantification. *Journal of Sensors* 2018 6564158.

[5] In, V. and Palacios, A. (2018). Energy Harvesting. In *Symmetry in Complex Network Systems*, Springer, Berlin - Heidelberg (DE) 295-316.

[6] Smilek, J. and Hadas, Z. (2018). Experimental evaluation of Tusi couple based energy harvester for scavenging power from human motion. *MATEC Web of Conferences* 211 05004.

[7] Liu, H., Zhong, J., Lee, C., Lee, S.-W. and Lin, L. (2018). A comprehensive review on piezoelectric energy harvesting technology: Materials, mechanisms, and applications. *Applied Physics Reviews* 5 041306.

[8] Erturk, A. and Inman, D. J. (2009). An experimentally validated bimorph cantilever model for piezoelectric energy harvesting from base excitations. *Smart Materials and Structures* 18*(2)* 025009.

[9] Benasciutti, D., Moro, L., Zelenika, S. and Brusa, E. (2010). Vibration energy scavenging via piezoelectric bimorphs of optimized shapes. *Microsystem Technologies* 16*(5)* 657-68.

[10] Gljušćić, P., Zelenika, S. and Franulović, M. (2019) Miniaturized wearable broadband energy harvesters. In *36th Danubia-Adria Symposium on Advances in Experimental Mechanics* Plzen (CZ) 17-8.

[11] Gljušćić, P. and Zelenika, S. (2020). Assessment of performances of optimized piezoelectric energy harvesters for wearables. In *20th EUSPEN International Conference* 49-52.

[12] Gljušćić, P., Zelenika, S. and Kamenar, E. (2018). Characterisation of Performances of Thermoelectric Generators for Energy Harvesting Applications. In *29th DAAAM International Symposium* Zadar (HR) 25-30.

Marko Perčić,[1, 2, 3] *Saša Zelenika*[1, 2, 3] *and Igor Mezić*[2, 4]

Characterization of influential parameters on friction in the nanometric domain using experimental and machine learning methods

[1] University of Rijeka, Faculty of Engineering, Vukovarska 58, 51000 Rijeka, CROATIA
[2] University of Rijeka, Centre for Micro- and Nanosciences and Technologies, Radmile Matejčić 2, 51000 Rijeka, CROATIA
[3] University of Rijeka, Center for Artificial Intelligence and Cybersecurity, Radmile Matejčić 2, 51000 Rijeka, CROATIA
[4] UC Santa Barbara, Department of Mechanical Engineering, Santa Barbara, CA 93105, USA

Abstract

Friction is a ubiquitous phenomenon of great research interest in engineering practice. Fundamental frictional features of two solids in contact and in relative motion are governed by microscopic single asperity contacts at their interface. A structured multidisciplinary approach to the experimental determination of friction in the nanometric domain is presented in this work. The dependence of nanoscale friction on process parameters comprising the materials in relative motion, normal forces, sliding velocities and the temperature conditions is studied experimentally by employing scanning probe microscopy. The data hence attained from multidimensional experimental measurements on thin-film samples is used for the development of machine learning-based models. In fact, due to the stochastic nature of the considered phenomena, conventional regression methods yield poor predictive performances, prompting thus the usage of the machine learning numerical paradigm. Such an approach enables obtaining an insight into the concurrent influence of the process parameters on nanoscale friction. A comparative study allows thus showing that, while the best typical regression models result in coefficients of determination (R^2) of the order of 0.3, the predictive performances of the used machine learning models, depending on the considered sample, yield R^2 in the range from 0.54 to 0.9. The proposed method, aimed at accomplishing an in-depth insight into the physical phenomena influencing nanoscale frictional interactions, will be complemented next with advanced studies based on genetic programming-based artificial intelligence methods. These could, in fact, allow obtaining a functional description of the dependence of nanoscale friction on the studied variable parameters, thus enabling not only true nanoscale friction prediction but also an important tool for control purposes.

Keywords: *nanoscale friction, experimental methodology, scanning probe microscopy, thin films, data mining, machine learning, artificial intelligence*

1. Introduction

Devices characterised by micro- and nanopositioning precision are often required in precision engineering as well as in micro- and nanosystems' technologies. When conventional devices based on sliding and rolling mechanisms are used in this frame, positioning precision is mostly limited by friction with its stochastic nonlinear characteristics [1]. Frictional phenomena on the macro- and meso-scales are described quite well in prior art, enabling their effects to be simulated via suitable models, as well as proficiently compensated via proper control typologies [2-3]. On the other hand, however, the available friction models do not take into due account true nanometric motions or the scaling phenomena related to friction [4]. In fact, the understanding of friction at the level of atomic interactions was enabled only in the last 20 to 30 years by the availability of scanning probe microscopy (SPM) methods [5], which enable experimental investigations of frictional single-asperity contacts [6].

A structured multidimensional experimental approach is thus developed in this work to study the dependence of the nanoscale friction force F_f on different concurrently varying process parameters comprising the materials in relative motion, normal forces F_N, sliding velocities v and temperatures ϑ.

Technologies (NANORI) of the University of Rijeka, Croatia [8]. The data obtained on thin-film samples is then used for the development of machine learning-based nanoscale friction models with the aim of gaining a deeper insight into the physical phenomena that influence nanotribological interactions.

2. Experimental set-up

The used experimental procedure involves SPM in the lateral force microscopy (LFM) mode (Figure 2), enabling measurements on Al_2O_3 and TiO_2 thin-film samples synthesized via atomic layer deposition (ALD) [9] at the NANORI premises, as well as Al, MoS_2

Fig. 1. Bruker Dimension Icon SPM

and stainless steel X39CrMo17-1 thin-film samples synthetized by using pulsed laser deposition (PLD) [10] at the Institute of physics in Zagreb, Croatia. Lateral (transversal) scans are hence performed on 500 x 500 nm^2 surfaces of the analysed samples, inducing a torsion of the cantilever bearing the measurement tips [11]. The resulting voltages are converted to values of the lateral (transversal) force exerted on the sample by calibrating the mechanical behaviour of the probe itself by using multiple methods, comprising the calibration based on using the TGF11 calibration sample [12], finite element modelling (FEM) and analytical calculations [6]. It was hence established that calibration is strongly dependant on the actual dimensions of the cantilevers. Considering that these dimensions are in micrometric range, while the production process of the probes inherently prevents the achievement of uniform dimensions in the whole production batch, calibration generally constitutes a hard and tedious task [6].

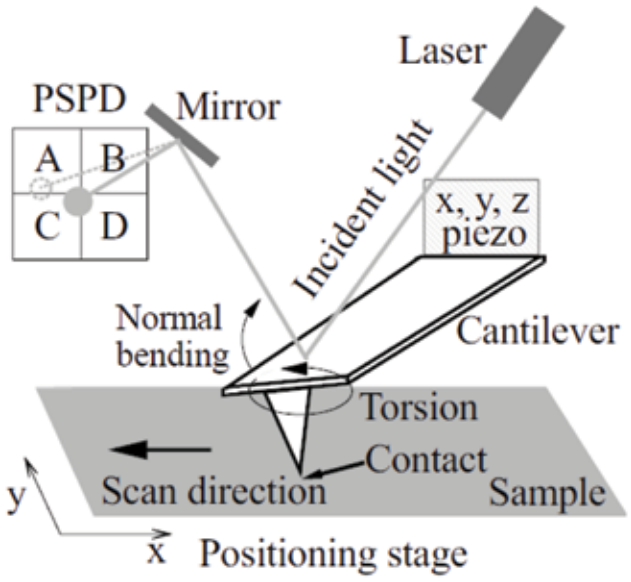

Fig. 2. Scheme of the LFM measurement configuration [6]

3. Definition of the measurement points

The considered parameters influencing nanoscale friction on the described samples, and their respective value ranges, are: normal force F_N = 10 nN… 150 nN, sliding velocity v = 5 nm/s … 500 nm/s and temperature ϑ = 20 °C … 80 °C. Design of experiment (DoE) is thus conducted by defining the experimental space via sampling methods that enable the development of a meta-model. Since recent studies indicate that, among these, centroidal Voronoi tessellation (CVT) [13] has several advantages, CVT is used to generate 50 sampling points in the considered multidimensional experimental space.

Given the set of desired points ("generators") and a distance function from each generator to its mass centroid, Voronoi tessellations are then subdivisions of the thus defined experimental space. The variation of the influencing parameters is herein defined via a discrete uniform distribution, i.e., a distribution where a finite number n of homogeneously spaced values has the same probability to be observed [13]. The integer parameters of the distribution are:

$$n = b - a + 1 \tag{1}$$

where a and b are the lower and upper limit of the values of the considered parameter.

A distribution of sample points is thus generated by a discrete probability distribution k attained by using a probability mass function $f(k)$ defined in equation (2). The cumulative distribution function $F(k)$, given by equation (3), is, in turn, used to specify the placement of the multivariate random variables (i.e., the points in the considered multidimensional influencing parameters' space):

$$f(k) = \begin{cases} 1/n & \text{if } a \le k \le b \\ 0 & \text{otherwise} \end{cases} \tag{2}$$

$$F(k) = \begin{cases} 0 & \text{if } k < a \\ \frac{[k]-a+1}{n} & \text{if } a \le k < b \\ 1 & \text{if } k > b \end{cases} \tag{3}$$

Given a density function, the centre of mass of each subset making up the Voronoi tessellation can thus be determined. Since, however, generally the locations of the generators do not coincide with the centres of mass of the data subsets, distinct Voronoi tessellations called CVTs are used to assure the convergence of these locations [13].

To gain insight into the stochasticity of the measured friction coefficients, five repetitive LFM measurements

are then performed in each of the 50 measurement points defined via the above DoE procedure [6].

4. Experimental results

Besides calibration, the inherent difficulties in the considered measurement procedure are amplified by synergetic effects occurring in the nanometric contact region, comprising the inevitable wear of the tip, thermal dilatations, and effects induced by the adhesive forces F_A. The latter proved to be especially tedious, since it has a strong nonlinear dependence on temperature on its own. It was hence determined that in the herein considered cases the correlation factor linking the LFM voltage readings to the corresponding nanoscale friction force values can vary by a whole order of magnitude. On the other hand, the wear of the used tips induces the necessity to use a fresh tip after every 50 LFM measurement cycles. The experimental methodology developed in this work in any case not only takes into account all these effects, but also limits their influence on measurements' uncertainties [6].

After taking into account the adhesion-corrected calibration factors, the obtained LFM scan signals are analysed in order to obtain the actual nanoscale friction force F_f in the 50 measurement points defined by employing the described CVT DoE methodology. The thus determined F_f values are shown, as typical result for the ALD and the PLD synthesized samples, in the colour-coded plots of Figure 3. In Figure 3a are thus depicted the results attained for the Al_2O_3, and in Figure 3b for the MoS_2 sample, respectively [6]. The results allowed also evidencing the noticeable stochastic nature of frictional phenomena, which makes the modelling based on this data, using conventional methods, difficult. The results allow establishing first-order rough correlations between the multiple studied influencing parameters and the resulting F_f values but, to determine systematic and reliable correlations, advanced mathematical tools have to be used [6].

5. Modelling nanoscale friction

Empirical insights obtained via the above thorough experimental procedure [6], are used as a basis for the development of a predictive model of nanoscale friction. The data collected in the 50 experimental measurement points, defined by employing the CVT DoE methodology, are hence used as the main dataset for the development of appropriate friction models. Each models' predictive performance is tested subsequently by employing the same experimental technique on a separate set of 15 measurement points defined randomly by using the Monte Carlo (MC) method [14].

Modelling is therefore primarily carried out using the conventional methods of regression analysis, i.e, linear, nonlinear, multivariate regression methods etc., but, due to the evidenced stochastic nature of the considered nanotribological phenomena, they yield poor results in describing the obtained experimental data, and even weaker predictive performances.

A machine learning (ML) paradigm is thus adopted to obtain an insight into the studied complex, multidimensional interactions and obtain a predictive model of nanoscale friction according to the schematics shown in Figure 4 [15]. Generally, ML algorithms for regression problems provide a so-called

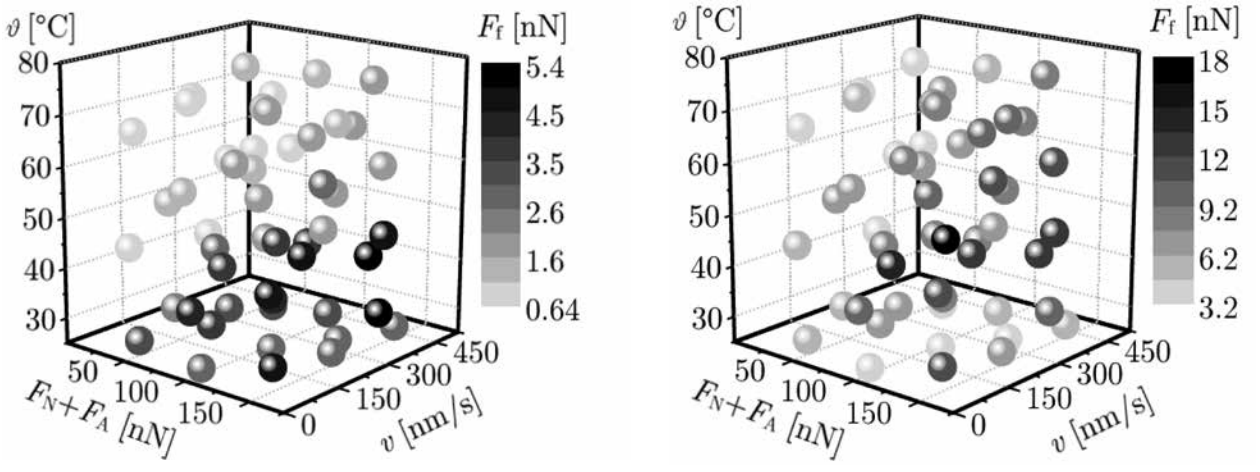

(a) (b)

Fig. 3. Colour-coded distributions of experimental F_f values for the 50 CVT DoE points for the Al_2O_3 (a), and MoS_2 (b) samples with adhesion-corrected total load F_N+F_A [6]

black-box solution with predictive results. The models thus developed are based on the TensorFlow [16], Scikit-learn [17] and GoSUMD [18] implementations. The herein used ML algorithms are thus additive regression, stacking and bagging classifiers, lazy algorithms, multi-layer perceptron (MLP), support vector regression (SVR), decision trees and random forest (RF) ensembles [19]. These methods are used for obtaining important insights into the analysed experimental space trough visualization analyses, providing important knowledge for further studies but, unfortunately, do not result in a functional mathematical form of the underlying relationships.

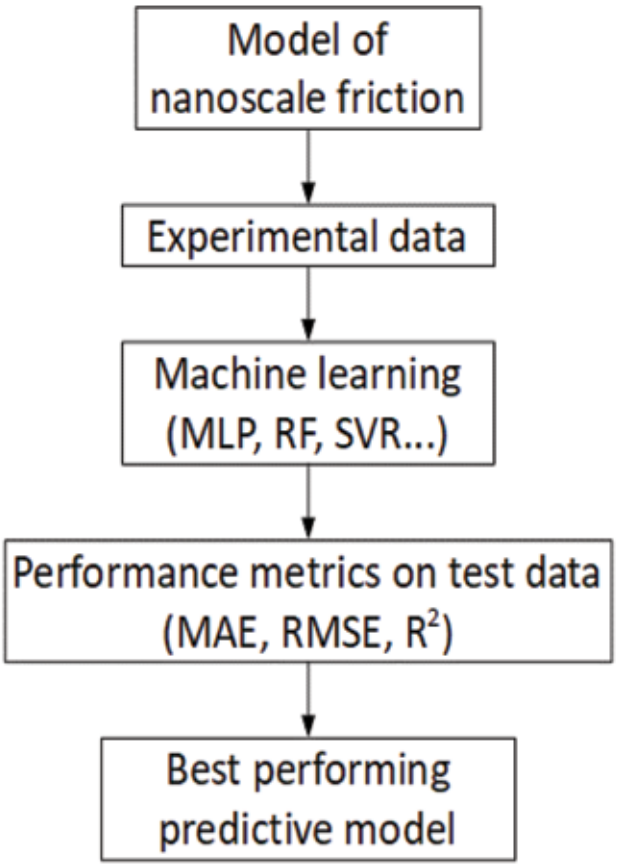

Fig. 4. Methodology for the development of ML-based predictive models of nanoscale friction

By employing binary encoding for the material class, the developed ML models are trained on the complete CVT-based dataset for each material separately, as well as on a combined (pooled) dataset pertaining to all studied materials, subjected in all cases to a 10-fold cross-validation. The ML models are then thoroughly assessed on the mentioned separately measured MC-based experimental dataset – the test dataset. To ensure realistic (habitual) conditions of the samples, these measurements are conducted, in contrast to the main CVT DoE-based measurements, without drying the samples prior to the measurements. Coupled to the

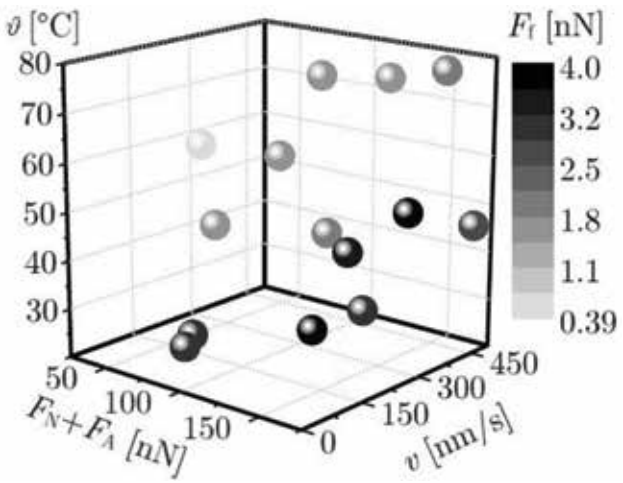

Fig. 5. Colour-coded distribution of experimental F_f values for the test dataset of 15 MC-based points for Al_2O_3 [15]

random distribution of the 15-point test dataset, the thus performed measurements, shown in Figure 5 for the Al_2O_3 thin-film sample, assure thus truthful F_f values that provide, moreover, the most difficult predictive task for developed models.

Each models' predictive performances are finally analysed by using performance metrics consisting of the mean absolute (MAE) as well as root mean square (RMSE) errors, and the respective coefficients of determination (R^2) [15].

6. Results and discussion

All developed ML models show far better predictive performance (higher R^2) than the conventional regression methods that yield R^2 in the range of ca. 0.3. What is more, all ML models, developed by training on a pooled (combined) dataset, comprising data acquired experimentally on multiple samples, show a higher level of predictive performances.

The finally obtained predictive performances on the MC-based test dataset are shown in Figure 6 for each of the best performing developed ML model. The respective R^2 values are reported in the Figure in parenthesis. In Figure 6 are depicted also the attained uncertainty levels in three shades of grey, representing, respectively, the variance of data ($\pm 1\sigma$ as the darkest, $\pm 2\sigma$ as the medium and $\pm 3\sigma$ as the lightest shade of grey that presents, with empirical near-certainty, all data).

For the Al_2O_3 thin-film sample synthesized via the ALD technique, in Figure 6a it can thus be evidenced that, even though the MLP algorithm results in high R^2

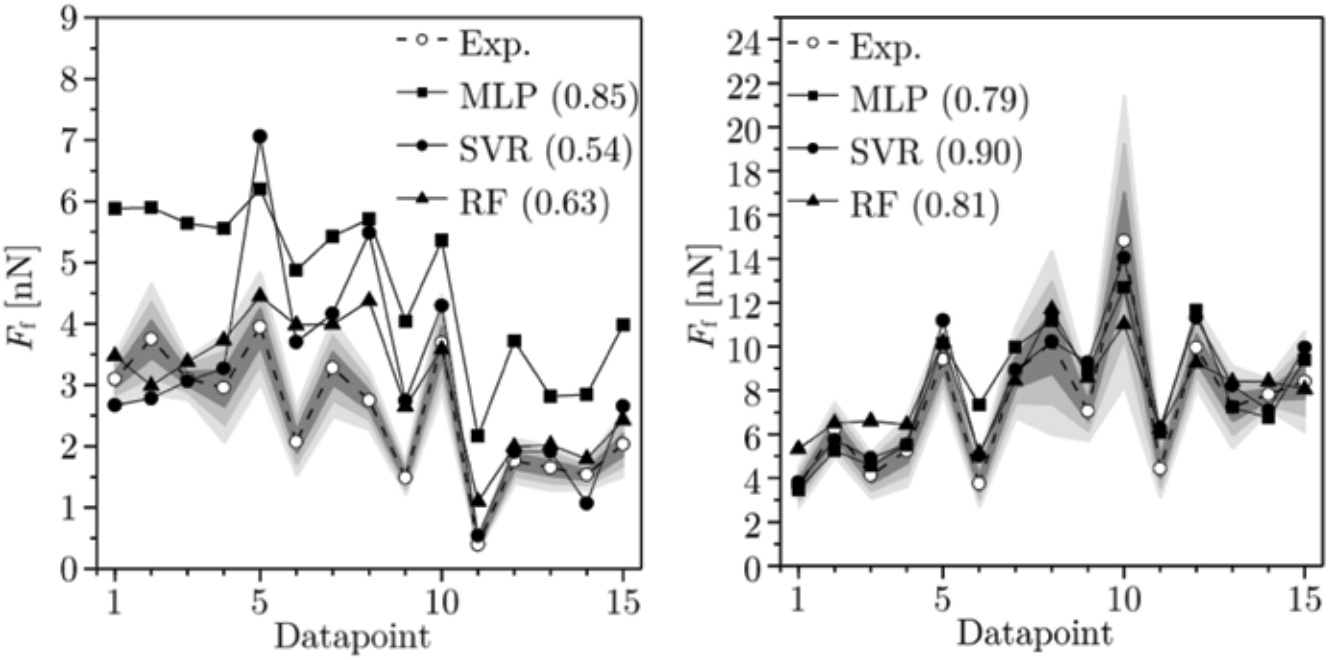

(a) (b)

Fig. 6. Predictive performances of the considered ML models on the MC test dataset for the Al_2O_3 (a), and MoS_2 (b) samples [15]

values, it is visually far quite far away from the experimental data. The RF and SVR predictions follow, in turn, the experimentally obtained data much better. In the case of the MoS_2 sample synthetized by using the PLD methodology, the test data predictions shown in Figure 6b allow noting much better predictive performances for all the ML models. The SVR algorithm captures in this case 90 % of the variance of F_f.

Such considerations allowed, therefore, concluding that the developed ML models allow providing effective predictions of the influence of the multiple concurrently acting process parameter on the value of the friction force with satisfactory levels of accuracy, i.e., with R^2 values ranging from a minimum 0.54 for the SVR algorithm on the Al_2O_3 sample, to a maximal value of 0.9 for the SVR prediction on the MoS_2 sample.

Although the developed ML models provide, thus, generally good predictive performance, their practical usage is quite limited by their inherent black-box nature. Further research has thus to be focused on obtaining models that allow obtaining mathematical expressions which will have equally good (or better) predictive performance as the ML models, but will enable practical usage in developing suitable control typologies that will allow an active compensation of nanotribological effects.

7. Conclusions and outlook

The activities and topics described in this work provide an overview of the obtained experimental and numerical results in the ongoing research effort on frictional phenomena in the nanometric domain carried on at the University of Rijeka, Croatia. The developed experimental methodology allows for the first time to determine the concurrent influence of multiple variable process parameters on the value of the nanoscale friction force.

The attained measurement results imply, however, the necessity of developing also suitable mathematical modelling tools, since the multidimensionality and the stochastic nature of the studied phenomena are an evident challenge for the conventional modelling methods. The analysis of the obtained measurements is thus performed by using state-of-the-art black-box ML models. It is hence established that their predictive performances can generally be considered satisfactory, but their practical applicability is limited, since they do not allow to obtain explicit functional dependencies of nanoscale friction on the multiple considered variable process parameters.

Further numerical analyses, based on employing novel genetic programming-based artificial intelligence (AI) methods are hence needed to fully characterize the influencing effects of nanoscale friction through a mathematical expression. Preliminary results obtained

in this frame are comforting since, despite the evidenced complexity of the herein studied phenomena, the AI-based symbolic regression models [20] could allow attaining excellent predictive performances, but indeed result also in a simple functional description of the multidimensional dependence of nanoscale friction on the studied variable influencing parameters. An operational and efficient tool for nanoscale friction prediction, for further scientific and technological analyses, but also for eventually enabling the compensation of frictional effects via appropriate adaptive control typologies, could thus be on the verge of being successfully obtained.

What is more, further studies on the considered topics are focused on bridging the multiscale gap in tribological studies, ranging from atomic and molecular to micro- and macroscales. To provide further and deeper insights into the fundamental principles of friction, the current efforts of our research group are therefore also directed towards active cooperation with the Molecular biology and nanotechnology laboratory (MoIBNL) at the University of Trieste, Italy, [21] on molecular dynamic studies of nanoscale friction phenomena.

Acknowledgements

This work is partly enabled by using the equipment funded via the EU European Regional Development Fund project no. RC.2.2.06-0001: "Research Infrastructure for Campus-based Laboratories at the University of Rijeka (RISK)" and supported by the University of Rijeka, Croatia, project uniri-tehnic-18-32 "Advanced mechatronics devices for smart technological solutions".

References

[1] Bhushan, Bh. (ed.) (2010). *Springer Handbook of Nanotechnology.* Springer, Berlin - Heidelberg (DE).

[2] Kamenar, E. and Zelenika, S. (2017). Nanometric positioning accuracy in the presence of presliding and sliding friction: Modelling, identification and compensation *Mechanics based design of structures and machines* 45*(1)* 111-26.

[3] Amthor, A., Zschaeck, S. and Ament, C. (2010). High Precision Position Control Using an Adaptive Friction Compensation Approach. *IEEE Transactions on Automatic Control* 55*(1)* 274-8.

[4] Luan, B. and Robbins, M. O. (2005). The breakdown of continuum models for mechanical contacts. *Nature* 435*(7044)* 929-32.

[5] Bhushan, Bh. (ed.) (2013). *Scanning Probe Microscopy in Nanoscience and Nanotechnology 3,* Springer, Berlin - Heidelberg (DE).

[6] Perčić, M., Zelenika, S., Mezić, I., Peter, R. and Krstulović, N. (2020). An experimental methodology for the concurrent characterization of multiple parameters influencing nanoscale friction. *Friction* 8*(3)* 577-93.

[7] University of Rijeka, Croatia. Equipment of the Centre for Micro- and Nanosciences and Technologies. Available on http://nanori.uniri.hr/wp-content/uploads/2018/04/Katalog-CMNZT_ENG.pdf (accessed on October 20, 2020).

[8] University of Rijeka, Croatia. Centre for Micro- and Nanosciences and Technologies: http://nanori.uniri.hr/ (accessed on October 21, 2020).

[9] Johnson, R. W., Hultqvist, A. and Bent, S. F. (2014). A brief review of atomic layer deposition: from fundamentals to applications. *Materials Today* 17*(5)* 236-46.

[10] Voevodin, A. A., Zabinski, J. S. and Jones J. G. (2007). Pulsed Laser Deposition of Tribological Coatings. In *Pulsed Laser Deposition of Thin Films* (Eason, R. ed.). John Wiley & Sons, Hoboken (NJ, USA) 585-609.

[11] Bhushan, Bh. (ed.) (2011). *Nanotribology and Nanomechanics II: Nanotribology, Biomimetics, and Industrial Applications,* Springer, Berlin - Heidelberg (DE).

[12] Varenberg, M., Etsion, I. and Halperin G. (2003). An improved wedge calibration method for lateral force in atomic force microscopy. *Review of Scientific Instruments* 74*(7)* 3362-7.

[13] Du, Q., Faber, V. and Gunzburger, M. (1999). Centroidal Voronoi Tessellations: Applications and Algorithms. *SIAM Review* 41*(4)* 637-76.

[14] Gentle, J. E. (2003). *Random Number Generation and Monte Carlo Methods – 2nd ed.* Springer-Verlag, New York (NY, USA).

[15] Perčić, M., Zelenika, S. and Mezić, I. (2020). A supervised machine learning approach to a predictive model of nanoscale friction. In *20th EUSPEN International Conference* 69-70.

[16] Abadi, M. et al. (2015). *TensorFlow:* Large-Scale Machine Learning on Heterogeneous Systems - software available from http://tensorflow.org.

[17] Pedregosa F. et al. (2011). Scikit-learn: Machine Learning in Python. *Journal of Machine Learning Research* 12 2825-30.

[18] AIMdyn System Analytics, Engineering Consulting and Software Development (2018). GoSUMD Software available from https://aimdyn.com/gosumd.

[19] Kecman V. (2001). *Learning and Soft Computing: Support Vector Machines, Neural Networks,* and Fuzzy Logic Models, MIT Press, Cambridge (MA, USA).

[20] Worzel. B. and Riolo, R. (eds.). (2003). *Genetic Programming Theory and Practice.* Springer, Boston (MA, USA).

[21] University of Trieste, Italy. Molecular Biology and Nanotechnology Laboratory: https://www.molbnl.it/ (accessed on October 29, 2020).

Report on the Euro-CASE 2020 conference

The Croatian Academy of Engineering (HATZ), as a long-term member of Euro-CASE, held the international scientific and professional annual conference Euro-CASE 2020 entitled "Dealing with Challenges of the European Energy Transition" on 20 November 2020.

The Euro-CASE 2020 Annual Conference, scheduled for June 2020, was postponed for November this year due to the coronavirus situation in Croatia and worldwide. In order to avoid social contacts, the conference was held on 20 November 2020 using Zoom application with technical support from the Euro-CASE and ATI Boards.

The annual Euro-CASE conference is the main professional and political forum organised by the member academies, bringing together leading European academics and experts to discuss the technical aspects of major issues. Through these annual conferences, Euro-CASE aims to maintain a leading role in promoting awareness of excellence in applied sciences and engineering and related issues of key importance to Europe. There is also a desire to ensure that the social effect of technological changes is duly taken into account, taking full consideration of environmental and sustainability aspects.

Sustainable energy production and use are one of the most important challenges of the 21st century. Providing a secure supply of clean, competitive and affordable energy for all presents complex technical, economic, social and political issues that need to be solved for sustainable development. At the Euro-CASE 2020 conference, the above-mentioned challenges were discussed in the context of the European energy transition.

The usual one-day Euro-CASE conference was shortened to a total of 3 hours of lectures and discussions on energy-related topics. The conference was divided into four parts: the introductory part, the first section, the second section and the time when participants could ask their questions in writing under the chat option. After the welcome speeches, the first section entitled "Energy Policies Challenges and Opportunity for Transformation" featured four invited lecturers, while the second section entitled "Implementation, Economic Impact and Challenges" featured five invited lecturers. The conference ended with questions and answers.

The conference was attended by 170 registered participants, which exceeded the expectations of the Academy Management and the Programme-Organising Committee. Out of a total of 23 national academies that make up Euro-CASE, the presidents or deputies of 21 academies attended the conference.

The conference sponsors were Croatian Electrical Power Industry (Hrvatska elektroprivreda d.d.) and the Croatian Vehicle Centre whereas the conference patrons were Croatian Chamber of Commerce and University of Zagreb.

The conference program, presentations of selected lecturers, and recordings of the entire conference can be found on the websites www.euro-case2020.com and www.hatz.hr.

Engineering Power – *Bulletin of the Croatian Academy of Engineering* Vol. 15(4) 2020 – ISSN 1331-7210

Publisher: Croatian Academy of Engineering (HATZ), 28 Kačić Street, P.O. Box 59, HR-10001 Zagreb, Republic of Croatia

Editor-in-Chief: Prof. Vladimir Andročec, Ph.D., President of the Academy retired Full Professor with tenure, University of Zagreb, Faculty of Civil Engineering

Editor: Prof. Zdravko Terze, Ph.D., Vice-President of the Academy University of Zagreb, Faculty of Mechanical Engineering and Naval Architecture

Guest-Editor: Prof. Saša Zelenika, Ph.D., University of Rijeka, Faculty of Engineering & Centre for Micro- and Nanosciences and Technologies

Activities Editor: Tanja Miškić Rogić

Editorial Board: Prof. Vladimir Andročec, Ph.D., Prof. Zdravko Terze, Ph.D., Prof. Slavko Krajcar, Ph.D.

Editorial Board Address: Croatian Academy of Engineering (HATZ), "Engineering Power" – Bulletin of the Croatian Academy of Engineering, Editorial Board, 28 Kačić Street, P.O. Box 59, HR-10001 Zagreb, Republic of Croatia

E-mail: hatz@hatz.hr

Graphical and Technical Editor: Minerva Graphica, Ltd., Zagreb

Proof-reader: Miroslav Horvatić, MA

Press: Tiskara Zelina, Ltd., Zelina

Circulation: 200